Article

7-MEOTA and 2-aminobenzothiazole heterodimers: structure-mechanism relationship of amyloid inhibitors based on rational design

Miroslav Gancar, Kiet Ho, S. Abdul Mohid, Nguyen Quoc Thai, Zuzana Bednarikova, H. Linh Nguyen, Anirban Bhunia, Eugenie Nepovimova, Mai Suan Li, and Zuzana Gazova

ACS Chem. Neurosci., **Just Accepted Manuscript** • DOI: 10.1021/acschemneuro.9b00419 • Publication Date (Web): 03 Feb 2020

Title: 7-MEOTA and 2-aminobenzothiazole heterodimers: structure-mechanism relationship of amyloid inhibitors based on rational design

Authors:

Miroslav Gancar[a+], Kiet Ho[b+], S. Abdul Mohid[c], Nguyen Quoc Thai[d], Zuzana Bednarikova[a], H. Linh Nguyen[b], Anirban Bhunia[c], Eugenie Nepovimova[e], Mai Suan Li[f*], Zuzana Gazova[a*]

Author Affiliation:

[a]Department of Biophysics, Institute of Experimental Physics Slovak Academy of Sciences, Watsonova 47, 040 01, Kosice, Slovakia

[b]Life Science Lab, Institute of Computational Science and Technology, Quang Trung Software City, Tan Chanh Hiep Ward, District 12, Ho Chi Minh City, Vietnam

[c]Department of Biophysics, Centenary Campus, Bose Institute, P-1/12, Ghose Bagan, CIT Road Scheme VIIM, West Bengal 700054, Kolkata, India

[d]Dong Thap University, 783 Pham Huu Lau Street, Ward 6, Cao Lanh City, Dong Thap, Vietnam

[e]Department of Chemistry, Faculty of Science, University of Hradec Kralove, Rokitanskeho 62, 500 03, Hradec Kralove, Czech Republic

[f]Institute of Physics, Polish Academy of Sciences, al. Lotnikow 32/46, 02-668, Warsaw, Poland

[+]These authors contributed equally

Corresponding Authors ([*]):

Zuzana Gazova, Department of Biophysics, Institute of Experimental Physics Slovak Academy of Sciences, Watsonova 47, 040 01, Kosice, Slovakia, gazova@saske.sk, Tel: +421 (055) 720 (4135)

Mai Suan Li, Institute of Physics, Polish Academy of Sciences, al. Lotnikow 32/46, 02-668, Warsaw, Poland, masli@ifpan.edu.pl, Tel: +(48 22) 843 70 01 (3326)

Keywords: protein aggregation**,** amyloid, heterodimerization, inhibition, lysozyme, small molecules

Abstract

The formation and accumulation of amyloid aggregates are the accompanying phenomena of amyloidoses, which are currently untreatable and include Alzheimer's and Parkinson's diseases, diabetes mellitus, non-neuropathic lysozyme systemic amyloidosis and others. One of the very promising therapeutic approaches seems to be inhibition of amyloid formation and/or clearance of amyloid aggregates. Small molecules have a great potential to interfere with amyloid fibrillation of poly/peptides, which can be improved by connection of cyclic structures into single multicyclic molecule and their dimerization. In our study, we focused on heterodimers consisting of 7-MEOTA and 2-aminobenzothiazole (BTZ) parent molecules connected by an aliphatic linker. Using *in vitro* and *in silico* methods, we investigated the ability of studied compounds to inhibit the amyloid aggregation of hen egg white lysozyme (HEWL). Heterodimerization led to significant improvement of inhibitory activity compared to parent molecules. Moreover, the efficiency of heterodimers varied; the most effective inhibitor contained the longest, eight carbon long linker. We suggest that binding of heterodimer to lysozyme blocks the interaction between β-domain and C-helix region essential for formation of amyloid cross-β structure. Prolongation of the linker ultimately enhances compounds ability to prevent this interaction by allowing the BTZ part of the heterodimer to bind more effectively, increasing compounds binding affinity, and also by greater steric obstruction. This study represents an important contribution for the recent rational design of potential lead small molecules with anti-amyloid properties and studied heterodimers are perspective candidates for the treatment of systemic lysozyme amyloidosis and other amyloid-related diseases.

Introduction

After decades of research, the protein amyloid aggregation still remains one of the biggest challenges for the scientific community due to their association with amyloid-related diseases as well as recently obtained knowledge that they also play physiological roles in organisms. Nowadays, it is believed all poly/peptide sequences can adopt the amyloid state under appropriate conditions[1]. Although the precise molecular mechanism of amyloid aggregation *in vivo* is still unknown there are a lot of factors affecting the propensity of poly/peptides to be transformed from a soluble state into almost insoluble amyloid structures. They include genetic mutations, post-translational modifications, high protein concentration, presence of metal ions and others[2]. *In vitro* exposure of proteins to amyloid inducing condition such as high temperature or protein concentration, pH and presence of salt or denaturants results in the formation of amyloid fibrils with cross-β architecture common to amyloid aggregates formed *in vivo.*

It is generally accepted that formation and accumulation of amyloid deposits in various tissues can have a toxic effect on different cell types leading to cell dysfunction. Amyloidoses, which represent a serious health problem leading to life-threatening organ failure and finally death[3]. Alzheimer´s and Parkinson´s diseases, the most common forms of dementia, as well as diabetes mellitus are some of the more than 50 currently known amyloid diseases. Human lysozyme is associated with lysozyme hereditary systemic non-neuropathic amyloidosis. It has been reported that amyloidogenic variants of the human lysozyme are encoded by six different mutations of the lysozyme gene. The phenotype of lysozyme systemic amyloidosis is heterogeneous and includes gastrointestinal symptoms, sicca syndrome, hepatic rupture, petechiae and purpura, renal failure and lymphadenopathy[4,5]. HEWL represents an interesting model system to investigate formation of amyloid aggregates and identify novel inhibitors with potential to deal with this disease. This 129 residues long anti-bacterial protein has been extensively used in studies as its structure and folding properties are well known and is highly homologous to human lysozyme. *In vitro*, it undergoes amyloid aggregation when exposed to high temperatures in acidic conditions[6,7].

Currently, there is no cure for amyloid diseases. Treatment is mainly focused on alleviating symptoms, thus improving the quality of patient's life. Therefore, the great emphasis is placed on the development of effective strategies for their successful treatment. One of the prospective therapeutic approaches is inhibition of amyloid fibrillization or clearance of amyloid aggregates.

Many small molecules proved to be capable of inhibition of the amyloid aggregation. Most of the studied compounds possess structural features known to be important for their interaction with core regions of early formed amyloid species and mature amyloid fibrils. These characteristics include the presence of aromatic rings, the substitution pattern of these aromatics and also the length and flexibility of the linker connecting the functional groups[8–10]. Curcumin and its derivatives exhibit the ability to interfere with β-amyloid fibrils and aggregates[8,11]. Derreumaux *et al*. reported effect of many drugs targeting mainly Aβ peptide obtained from *in vit*ro, *in vivo* experiments and clinical trials[12,13]. Glyco-acridines inhibit amyloid aggregation of human insulin as well as HEWL[14,15]. Siddiqi *et al*. shown that capreomycin effectively suppresses the insulin amyloid fibrillization[16]. The ability of polyphenols to affect the amyloid aggregation of HEWL *in vitro* has been reported[17].

Tacrine was the first cholinesterase inhibitor approved by FDA and also one of the most popular aromatic structures tested for possible anti-amyloid properties. However, it has been restricted due to its hepatotoxicity[18,19]. Therefore, the search for more effective, secure and multifunctional tacrine derivatives is still of interest[8]. It has been demonstrated that tacrine analogue 7-methoxytacrine (7-MEOTA) and its derivatives have the ability to inhibit the amyloid formation of $A\beta_{1-40}$ peptide while being less toxic and pharmacologically equally active to tacrine[19,20]. The other interesting molecule is benzothiazole and its derivatives, one of the most important chemical structures featured in a variety of natural and pharmaceutical agents[21].

Heterodimerization remains an attractive concept leading to preservation, combination or improvement of beneficial biological properties of parent compounds. It is believed that it is a valid concept when dealing with diseases as complex as amyloidoses. Furthermore, it brings up an opportunity to take advantage of the active linker region, which connects parent molecules and thus, enhance the effects of unique designed anti-amyloid compounds[9,22].

In this paper, we focus on the effect of hybrid heterodimers on amyloid aggregation of hen egg white lysozyme (HEWL). A novel series of heterodimers (HK compounds) was prepared through linkage of functional molecules 7-MEOTA and 2-aminobenzothiazole (BTZ) using aliphatic linker varying in length. The results obtained using various *in vitro* and *in silico* biophysical methods show that HK compounds are capable of effective dose-dependent inhibition of HEWL amyloid aggregation at acceptable toxicity levels. It was found that heterodimerization greatly improves the anti-amyloid ability of the parent compounds. Moreover, we investigated the structure-activity relationship of studied molecules. Binding of heterodimers to HEWL mostly depends on compound aromatic groups and leads to the

blocking of the interaction between β-domain and C-helix region essential for formation of amyloid cross-β structure. Despite this fact, the length of the linker is a decisive factor among the HK compounds in terms of their affinity to HEWL as well as their inhibitory activity.

Results and Discussion

Heterodimerization of small molecules represents a novel approach allowing to improve anti-amyloid activities of compounds. We synthetized heterodimeric 7-MEOTA – 2-aminobenzothiazole (BTZ) molecules (HK compounds 1066, 1068, 1070, 1072) by linkage of parent molecules 7-MEOTA and BTZ using length variable aliphatic linker (C_n; n = 2, 4, 6, 8). Chemical structures of compounds are displayed in Table 1. The parent molecules (7-MEOTA, BTZ) as well as four heterodimers were investigated to determine whether they are able to inhibit HEWL amyloid aggregation. *In vitro* and *in silico* experiments were used as well to examine their mechanism of action and to identify relationship between the molecular structure of heterodimers and their inhibitory activity.

Name	2D structure	3D structure
7-MEOTA	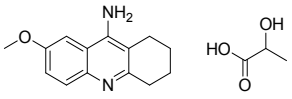	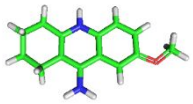
BTZ	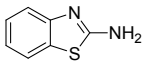	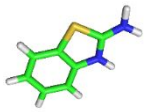
HK 1066	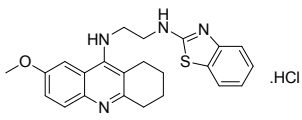	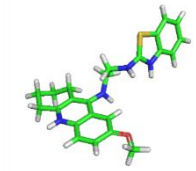
HK 1068	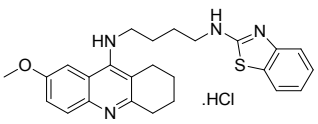	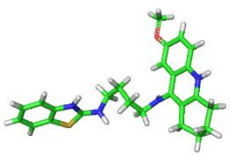

HK 1070	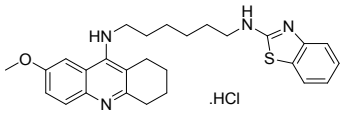	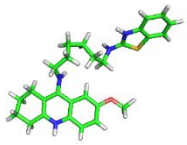
HK 1072	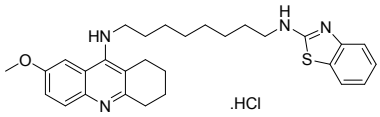	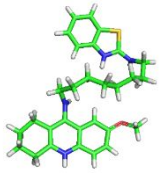

Table 1. 2D and 3D structures of studied parent molecules 7-MEOTA, BTZ and synthesized heterodimeric HK compounds.

Inhibition of HEWL amyloid fibrils formation and determination of IC_{50} values

The ability of studied compounds to inhibit amyloid aggregation of HEWL was examined using ThT fluorescence assay. The extent of inhibition of amyloid fibrillization was studied for all six compounds and an equimolar mixture of 7-MEOTA and BTZ at concentration gradient ranging from 100 pM to 1 mM and fixed 10 μM HEWL concentration. The relative fluorescence intensities normalized to fluorescence signal of HEWL amyloid fibrils alone (taken as 100 %) are presented in Figure 1. As a decrease in fluorescence indicates the

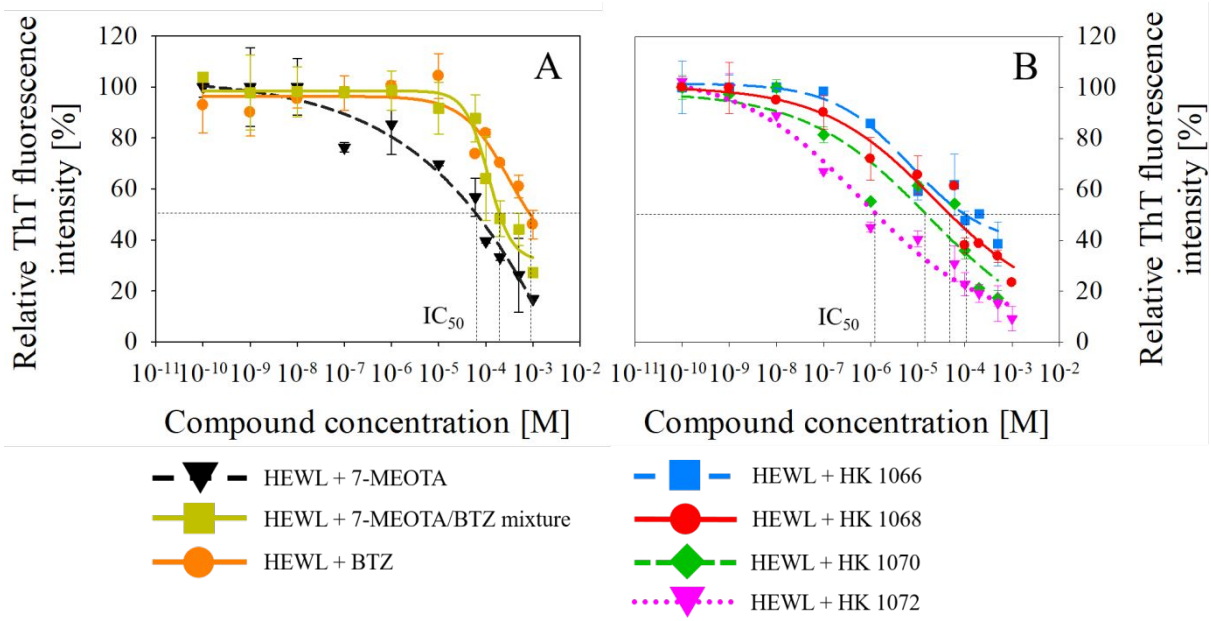

Figure 1. ThT fluorescence intensities of HEWL fibrillization in presence of increasing concentration of (A) 7-MEOTA (black triangles), BTZ (orange circles) and their equimolar

mixture (dark yellow squares); (B) HK 1066 (blue squares), HK 1068 (red circles), HK 1070 (green diamonds) and HK 1072 (magenta triangles). ThT fluorescence intensities were normalized to fluorescence of 10 μM HEWL fibrils formed without added compounds (taken as 100 %). Experiments were performed as three independent measurements (n = 3); error bars represent the average deviation of three separate samples.

ability of compounds to inhibit the amyloid fibrils formation, we can conclude that all studied compounds inhibit HEWL amyloid fibrillization to some extent. The efficiency is affected by compound concentration, heterodimerization of compounds and their structure.

A concentration gradient of 7-MEOTA resulted in a steady decline of ThT fluorescence intensity starting at 100 nM concentration (Figure 1, black triangles). Regarding BTZ (Figure 1, orange circles) and an equimolar mixture of parent molecules (Figure 1, dark yellow triangles) we observed a steep decline of ThT fluorescence intensity starting from the ~ 80 μM concentration. Moreover, an equimolar mixture had worse efficiency than 7-MEOTA alone, suggesting a competitive binding of parent molecules. At the highest used concentration (1 mM) the fluorescence intensity reached ~ 15 % for 7-MEOTA, ~ 40 % for BTZ and ~ 30 % for their mixture of the signal observed for untreated HEWL amyloid fibrils. That corresponds to ~ 85 %, ~ 60 % and 70 % inhibitory activity for 7-MEOTA, BTZ and their mixture, respectively.

On the other hand, data collected for heterodimer HK 1072 (Figure 1B, magenta triangles) show a steady decline of ThT fluorescence with increasing compound concentration starting from the picomolar region. At the highest (1 mM) concentration only ~ 10 % fluorescence signal was observed in comparison to fluorescence detected for untreated lysozyme fibrils. It corresponds to ~ 90 % inhibition of HEWL amyloid aggregation. The inhibitory activity slightly decreased for compounds with shorter linkers, namely ~ 80 % for HK 1070 compound (Figure 1B, green prisms) and ~ 75 % for HK 1068 (Figure 1B, red circles).The compound HK 1066 (Fig. 1B, blue squares), the heterodimer with shortest, only two carbons long linker, inhibits HEWL amyloid aggregation by roughly 60 %.

Overall, the obtained data suggest that inhibitory activity of parent molecules 7-MEOTA, BTZ and their mixture without heterodimerization is significantly lower in comparison to the heterodimers. Moreover, the effect of linker length on the inhibitory activity of amyloid aggregation of HEWL was observed. The data presented in Figure 1B suggest that prolongation of the linker had a positive effect on compounds capability to suppress amyloid aggregation of HEWL. The highest inhibition was observed for compound HK 1072 with

longest, eight carbon long linker. The gradual decline in inhibitory activity was observed for heterodimers with a shorter linker length. For better quantification of inhibitory properties of studied compounds, the fluorescence intensity values were fitted. The obtained curves were used for calculation of IC_{50} values (half-maximal inhibitory concentrations of compounds), which are summarized in Table 2. BTZ has shown the lowest inhibitory potential with the highest IC_{50} value equal to 871 μM. The second parent molecule, 7-MEOTA, exhibited better anti-amyloid properties with IC_{50} ~ 67 μM. Their equimolar mixture had higher IC_{50} value than all heterodimers, equal to 196.7 μM. Importantly, all heterodimers with exception of HK 1066 were more effective at inhibiting HEWL amyloid aggregation than parent molecules BTZ, 7-MEOTA or their equimolar mixture. Moreover, it was found that with prolonging aliphatic linker of heterodimers the inhibitory efficiency of compounds increased in correspondence to decline of their IC_{50} values. The most effective compound was heterodimer HK 1072 with IC_{50} ~ 1.6 μM, which is two orders of magnitude better than BTZ and one order enhancement in comparison to 7-MEOTA. The obtained results suggest that both the heterodimerization and linker length are important factors determining compounds inhibitory ability.

Table 2. IC_{50} values of 7-MEOTA, BTZ, their equimolar mixture and HK compounds corresponding to their ability to inhibit amyloid aggregation of HEWL. Data represent the mean value obtained from three independent measurements and an average deviation.

Compound	**IC_{50} [μM]**
7-MEOTA	66.8 ± 4.4
BTZ	871.4 ± 64.3
eq. mixture 7-MEOTA:BTZ	196.7 ± 16.5
HK 1066	115.6 ± 11.3
HK 1068	48.7 ± 7.6
HK 1070	15.4 ± 0.9
HK 1072	1.6 ± 0.3

Morphology of amyloid aggregates

Atomic force microscopy (AFM) was used to visualize morphological changes of HEWL amyloid fibrils forming in the presence of studied compounds (Figure 2).

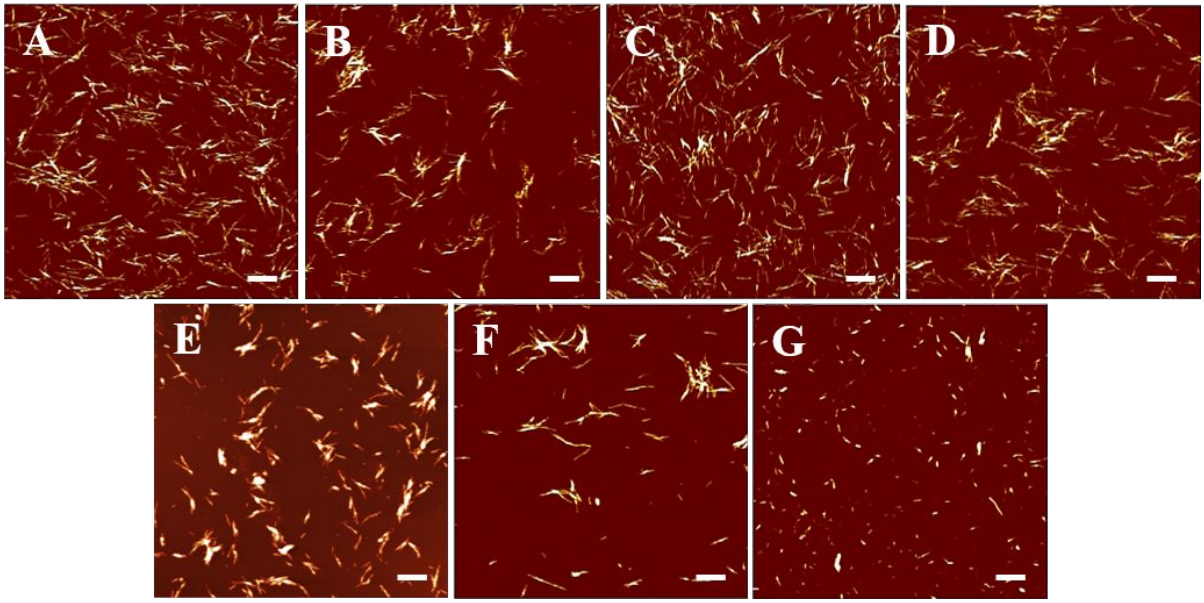

Figure 2. AFM images of HEWL fibrils formed alone (A) or in a presence of studied compounds 7-MEOTA (B), BTZ (C), HK 1066 (D), HK 1068 (E), HK 1070 (F) and HK 1072 (G). The concentration of HEWL was 10 μM and the concentration of added compounds was 500 μM. Bars represent 1 μm.

For BTZ (Figure 2C) the quantity and morphology of amyloid fibrils was comparable to HEWL amyloid aggregates formed alone, confirming very low inhibitory activity of this compound (Figure 2A). The reduction of the amount of amyloid aggregates was detected for lysozyme fibrillization in the presence of compound 7-MEOTA (Figure 2B). Among the heterodimers, the lowest amount reduction of the amyloid fibrils was observed for HEWL fibrillization in the presence of HK 1066 (Figure 2D) corresponding to its higher IC_{50} value. Addition of HK 1068 (Figure 2E) caused similar morphology and quantity changes as were observed for 7-MEOTA. Considerably fewer aggregates were formed in the presence of compound HK 1070 (Fig. 2F) and aggregates formed in the presence of HK 1072 (Figure 2G) in particular appeared much shorter and more amorphous compared to other samples. AFM images of formed aggregates are in a very good correlation with calculated IC_{50} values and support results obtained from ThT fluorescent assay.

Secondary structure determination - ATR FTIR spectroscopy

In order to analyze differences in the content of secondary structure of HEWL amyloid fibrils formed alone and in the presence of studied compounds, samples were examined using ATR FTIR spectroscopy. The FTIR spectra recorded for native and untreated HEWL amyloid fibrils as well as for lysozyme aggregates formed in the presence of parent molecules BTZ, 7-MEOTA and heterodimers HK 1068 (representing compounds with the short linker) and HK 1072 (compound with the longest linker and the best inhibitory activity) are presented in Figure 3A. The spectra were deconvolved (Figure S1) to calculate the particular protein secondary structures (Table S1). The content of α-helical and β-sheet content has been determined for all samples is presented in Figure 3B.

The absorption spectrum of native HEWL in the amide I region (Figure 3A, green

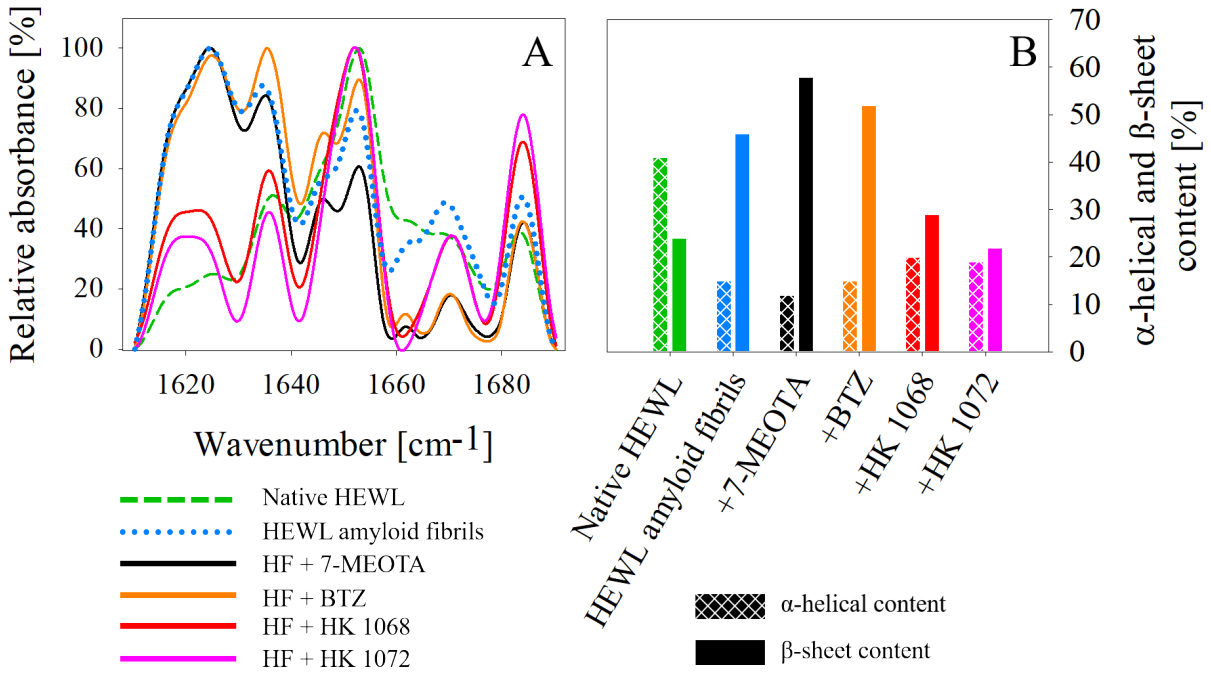

Figure 3. (A) ATR FTIR spectra of native 50 μM HEWL (green dashed line) and 50 μM HEWL amyloid fibrils after fibrillization without added compound (blue dotted line) or in presence of 500 μM compound BTZ (orange line), 7-MEOTA (black line), HK 1068 (red line) and HK 1072 (magenta line). (B) α-helical (patterned columns) and β-sheet (full-colored columns) content determined for native HEWL, HEWL fibrils and HEWL fibrillized in presence of compounds BTZ, 7-MEOTA, HK 1068 and HK 1072. The resulting FTIR spectra represent an average of 254 repetitions.

dashed line) shows a wide bands at 1653 cm^{-1} and 1661 cm^{-1} corresponding to ~ 41 % α-helical content (Fig. 3B, green patterned column), which is in agreement with other studies[23]. Bands at 1625 $cm^{-1}$and 1636 cm^{-1} represent ~ 24 % β-sheet content (Fig. 3B, green full-color column). Contrary, HEWL amyloid fibrils formed alone (Fig. 3A, blue dotted line) have bands at 1624 cm^{-1} and 1636 cm^{-1} indicating a significant increase in β-sheet content, characteristic for HEWL amyloid fibrils[4]. Calculated β-sheet content for HEWL amyloid fibrils was ~ 46 % (Fig. 3B, blue full-color column). This significant increase was mainly at the expense of lower α-helical content in HEWL amyloid fibrils (~ 15 %) (Figure 3B, blue patterned column).

An addition of studied parent molecules BTZ (Figure 3A, orange line) and 7-MEOTA (Figure 3A, black line) led to slight changes in spectra compared to the spectrum detected for HEWL fibrils and interestingly, the β-sheet content was higher (58 % for 7-MEOTA and 52 % for BTZ) (Figure 3B, black and orange full-color columns) as we observed for lysozyme fibrils alone (46 %). An effect of heterodimers HK 1068 and HK 1072 on the secondary structure content of HEWL amyloid aggregates was much more significant. Bands at 1623 and 1636 cm^{-1} (Figure 3A, red and magenta line) related to the β-sheet secondary structure were still observed, however at much lower intensity. The spectra deconvolution (Figure 3B, red and magenta full-colored columns) determined ~ 29 % and ~ 22 % β-sheet structure content for HK 1068 and HK 1072, respectively. Interestingly, the observed decrease in β-sheet content in comparison to HEWL amyloid fibrils prepared alone was mostly at cost of an extensive increase of random coil (~ 10 %), β-turn content (~ 4 - 10 %) and a minor increase of the α-helical structures (~ 5 %). These results indicate that heterodimers HK 1068 and HK 1072 were able to prevent the formation of cross-β structures unique for amyloid fibrils, while also conserving part of α-helical structure. The content of secondary structures is shown in the supporting information (SI) (Figure S1, Table S1).

Docking results

In docking simulation, a 40 x 45 x 50 $Å^3$ box with the center of mass at (-1.74, 0.06, -9.33) Å was used. Binding location of 6 studied compounds in HEWL is shown in Figure 4. All compounds have almost the same binding position with 5 common residues: Trp63, Asn59, Asp52, Gln57, and Ala107. More detailed information about the ligands in the binding pocket is summarized in Table S2 and Figure S2 in SI.

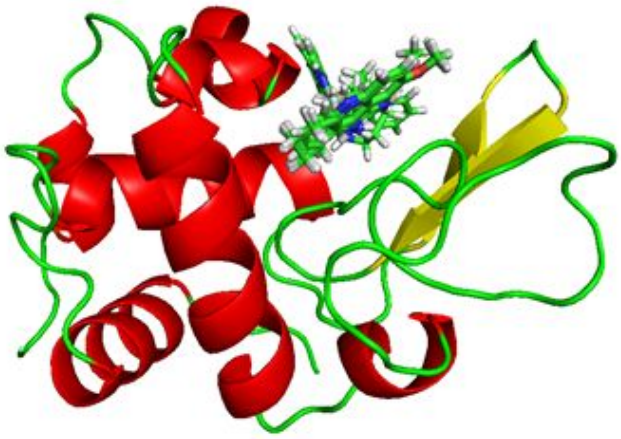

Figure 4. The binding site of 6 studied compounds in HEWL.

Contact networks determined for studied compounds in the best docking mode are shown in Figures S3 and S4. Except for the compound HK 1070, which forms 1 hydrogen bond (HB) with Asn46 no other compounds develop hydrogen bonds with HEWL, indicating that HBs do not prevail in the binding affinity of HK compounds. The number of non-bonded contacts (NBCs) is 7, 9, 13, 14, 12, and 11 for BTZ, 7-MEOTA and heterodimers HK 1066, HK 1068, HK 1070, HK 1072, respectively (Table S3, Figures S3 and S4). Compound HK 1066 has the highest number of NBCs (14) and, therefore, it has the highest binding affinity ΔE_{bind} = -8.7 kcal.mol^{-1}. The BTZ compound with the fewest number of NBCs has the worst binding affinity, ΔE_{bind} = -5.7 kcal.mol^{-1}. Thus, the NBC network is superior to the HB network in terms of the binding affinity of HK compounds. The binding affinity of all compounds is also summarized in Table S3. The correlation between ΔE_{bind} and IC_{50} values is high with the correlation level R = 0.78 (Figure S5).

MM-PBSA result: Binding free energy

Because results from molecular docking are not sufficiently reliable, we estimated the binding free energy using molecular dynamics (MD) simulation and the MM-PBSA method. For each receptor-ligand complex, we performed five independent 100 ns MD runs starting from the same starting configuration, obtained in the best docking mode (Figure 4), but with different random seed numbers to create different initial velocities. In order to estimate the equilibration time τ_{eq}, we controlled the time dependence of RMSD assuming that equilibrium was reached if this dependence gets saturated. Apparently, τ_{eq} depends on the compound and the trajectory ranging from 40 to 60 ns (Figure S6). Snapshots collected at equilibrium represented by arrows in Figure S6 were used to compute ΔG_{bind} (Eq. (1)). The obtained data are presented in Table 3.

Table 3. The binding free energy (kcal.mol^{-1}) obtained by the MM-PBSA method. The experimental binding free energy was estimated using the equation $\Delta G_{exp} = RT\ln(IC_{50})$, where T = 300 K, the gas constant R = 1.987.10^{-3}kcal K^{-1}mol^{-1}.

Ligand	ΔE_{elc}	ΔE_{vdW}	ΔG_{PB}	ΔG_{SA}	-TS	ΔG_{bind}	ΔG_{exp}
7-MEOTA	-25.1 ± 2.9	-21.2 ± 2.0	11.5 ± 3.6	-7.1 ± 0.4	24.3 ± 2.9	-17.6 ± 5.2	-5.7
BTZ	-13.6 ± 2.8	-14.8 ± 2.2	4.3 ± 1.7	-6.8 ± 0.2	23.3 ± 2.1	-7.4 ± 2.4	-4.2
HK 1066	-20.1 ± 7.4	-20.7 ± 3.7	6.2 ± 4.7	-7.4 ± 0.4	26.2 ± 2.9	-15.8 ± 3.2	-5.4
HK 1068	-14.2 ± 1.1	-28.4 ± 6.1	7.7 ± 2.1	-7.5 ± 0.4	23.8 ± 4.1	-18.7 ± 4.9	-5.7
HK 1070	-23.5 ± 9.6	-25.1 ± 8.0	6.4 ± 1.0	-7.1 ± 0.4	22.1 ± 3.3	-27.2 ± 4.7	-6.5
HK 1072	-24.3 ± 5.4	-31.2 ± 3.5	10.3 ± 2.1	-6.4 ± 0.4	19.2 ± 3.0	-32.5 ± 5.2	-7.9

The lowest ΔG_{bind} (-32.5 ± 5.2 kcal.mol^{-1}) was obtained for compound HK 1072, which is in correlation with the *in vitro* experiments, showing that this compound has the best inhibitory effect and the lowest IC_{50} value. The binding free energy calculated by the MM-PBSA method strongly correlates with the number of carbon atoms of the linker (Figure 5), as well as with IC_{50} values (Figure S7) and ΔG_{exp} (Figure S8). This means that the addition of the carbon linker leads to a stronger interaction between compounds and HEWL.

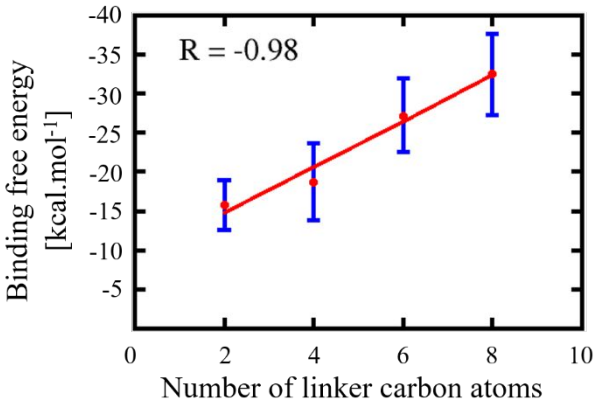

Figure 5. The correlation between binding free energy (MM-PBSA) and the number of linker carbon atoms. Error bars represent standard deviation.

To shed more light on the binding mechanism, HK compounds were divided into 3 structural blocks (Figure 6). The first block is a linker region, which consists of 2 (HK 1066), 4 (HK 1068), 6 (HK 1070) and 8 (HK 1072) carbon atoms. Therefore, block 1 has 6, 12, 18, 24 atoms for HK 1066, HK 1068, HK 1070, and HK 1072, respectively. The block 2 of 7-MEOTA has 33 atoms and block 3 of BTZ has 16 atoms.

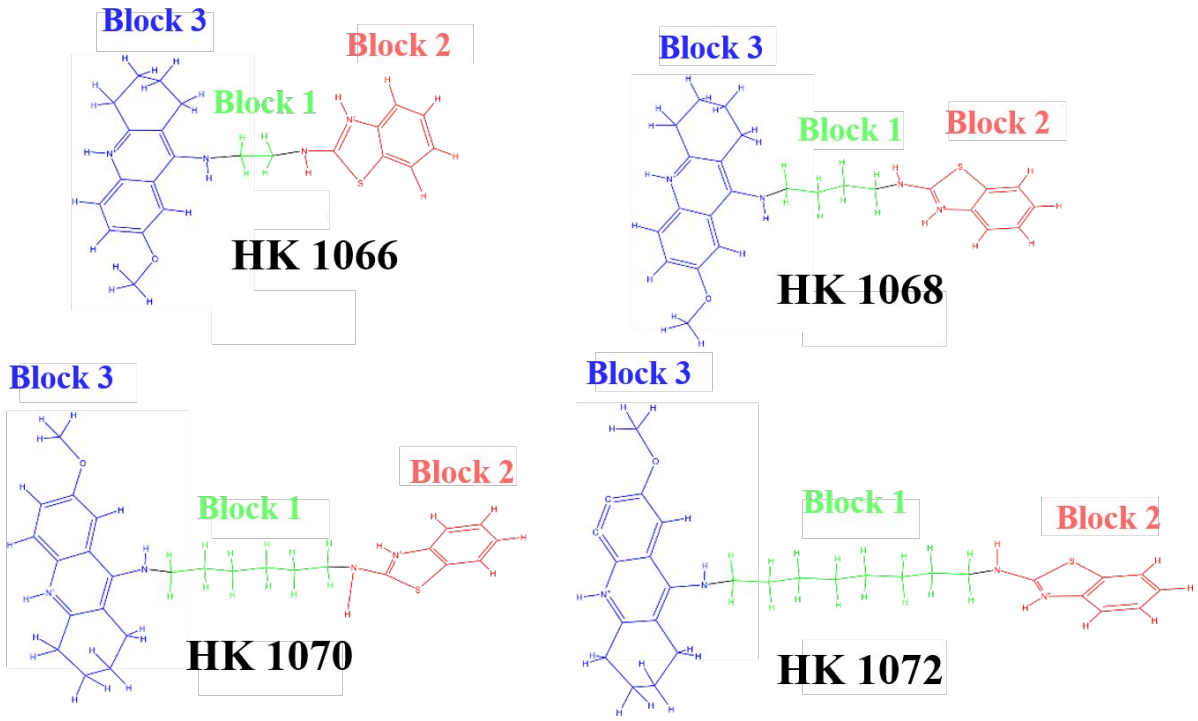

Figure 6. Three structural blocks of HK compounds. Block 1 represents aliphatic linker (green), block 2 corresponds to the first parent molecule BTZ (red) and block 3 is the second parent molecule 7-MEOTA (blue).

Contribution of block 1 varies and depends on the number of carbon atoms in the linker (Table 4). The vdW interaction of block 1 with the HEWL molecule greatly increases from

Table 4. Decomposition of the interaction energy (kcal.mol^{-1}) into 3 blocks

Ligand	Block 1		Block 2		Block 3	
	ΔE_{elc}	ΔE_{vdW}	ΔE_{elc}	ΔE_{vdW}	ΔE_{elc}	ΔE_{vdW}
HK 1066	-8.0	-1.8	-3.7	-15.3	-8.3	-3.6
HK 1068	-4.9	-4.5	-2.1	-17.4	-7.2	-6.6
HK 1070	-7.2	-4.9	-5.5	-13.9	-10.8	-6.3
HK 1072	-11.9	-9.3	-4.7	-15.6	-6.1	-5.4

-1.8 kcal.mol^{-1} to -10.0 kcal.mol^{-1}, whereas the contributions of block 2 and block 3 are almost equal. The contribution of block 2 to the vdW interaction is more important than that of the

other two blocks since it has more atoms (33 atoms). In general, block 1 contributes to the vdW interactions less than block 2, however, the overall trend is that the higher number of linker carbons, the stronger binding of the ligand to the HEWL molecule. Regarding electrostatic interactions, we observed fluctuations within an error, which correlates well considering the structures of parent molecules are identical and their binding positions are roughly the same.

Binding epitope of HEWL - small molecule interaction

Two-dimensional homonuclear NOESY experiment was done to elucidate the structural perturbation of HEWL in the presence of HK 1066 and HK 1072 at an equimolar ratio. Figure 7 depicts the superimposed spectra of HEWL in the absence and presence of ligands (HK 1066 and HK 1072), respectively. After careful investigation, several chemical shift perturbations (CSP) were observed in both cases; but HK 1066 has shown peak broadening effect against several amino acid residues such as Asp48, Asp52, Asn59, and Trp108 (Figure 7A). The same effect was also observed for CαH of Ile98 and CβHs of Gln57. On the contrary, in the presence of HK 1072 residues Asn59 and Trp108 (data not shown) showed a downfield CSP of ~ 0.06 and 0.02 ppm, respectively (Figure 7B). Other amino acid residues responsible for binding to HK 1072 as evidenced from the molecular docking analysis remained unchanged in the NOESY spectrum.

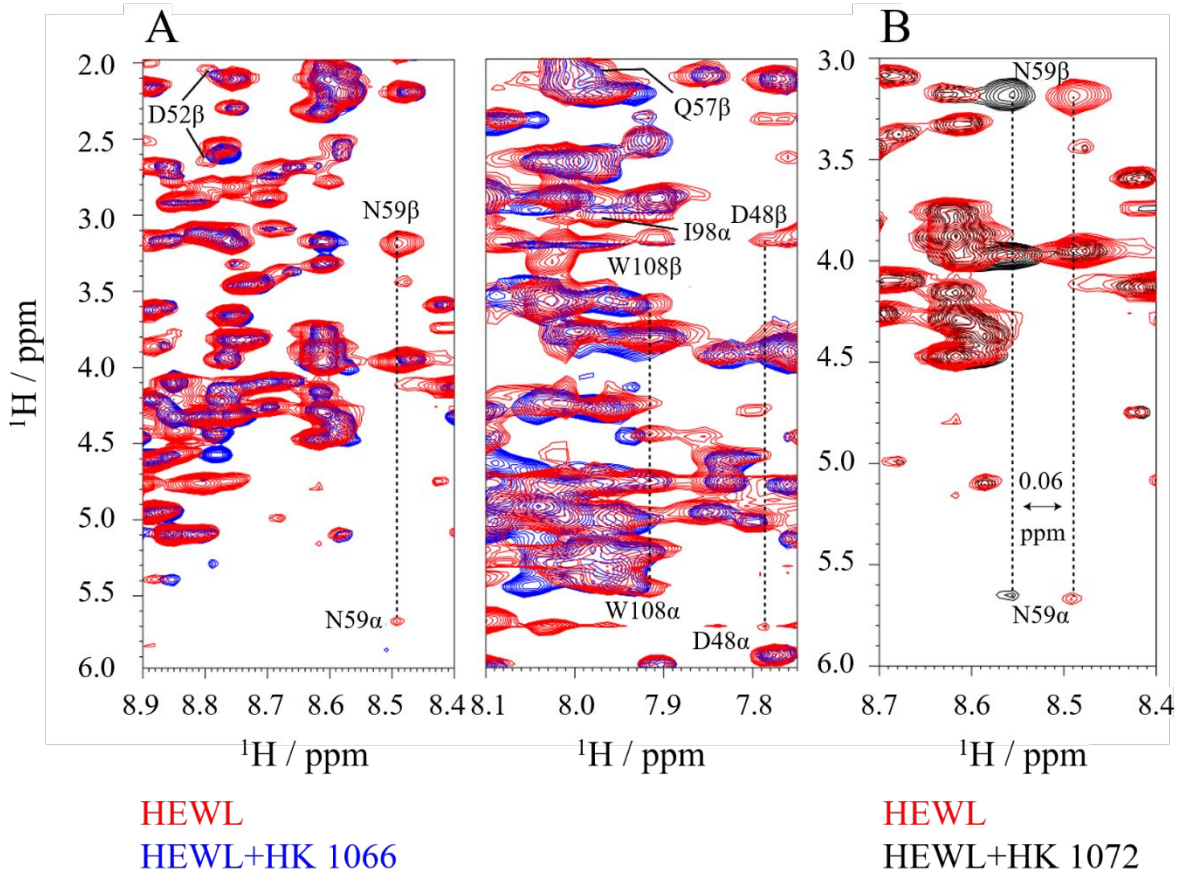

Figure 7: 2D NOESY spectra of free HEWL (red) and in the presence of (A) HK 1066 (blue) or (B) HK 1072 (black). The superimposed spectra confirm the residue-specific chemical shift changes. CSPs were obtained for several residues that are involved in binding with the ligands, which were also determined by the molecular docking.

Additionally, the remarkable CSPs were observed for the indole (NεH) ring protons of Trp62 and Trp111 of HEWL in the presence of the ligands, HK 1066 and HK 1072 (Fig. 8). Trp62 showed ~ 0.13 and 0.08 ppm downfield CSP for HK 1066 and HK 1072, respectively while Trp111 showed ~ 0.07 and 0.04 upfield CSPs after addition of equimolar concentration of HK1066 and HK1072, respectively (Figure 8A, B). It is noteworthy to mention that the Trp63 and Trp108 of HEWL have been shown to interact with the HK compounds in molecular docking analysis, but these residues showed minimal (in presence of HK 1066) to no (in presence of HK1072) CSP in the NOESY spectrum. Surprisingly, their neighboring residues, such as Trp62 and Trp111 showed significant chemical shift perturbation upon addition of the equimolar concentration of the HK ligands. Generally, aromatic-aromatic interaction along with hydrophobic stacking plays a crucial role to halt the amyloid aggregation of HEWL molecules[24].

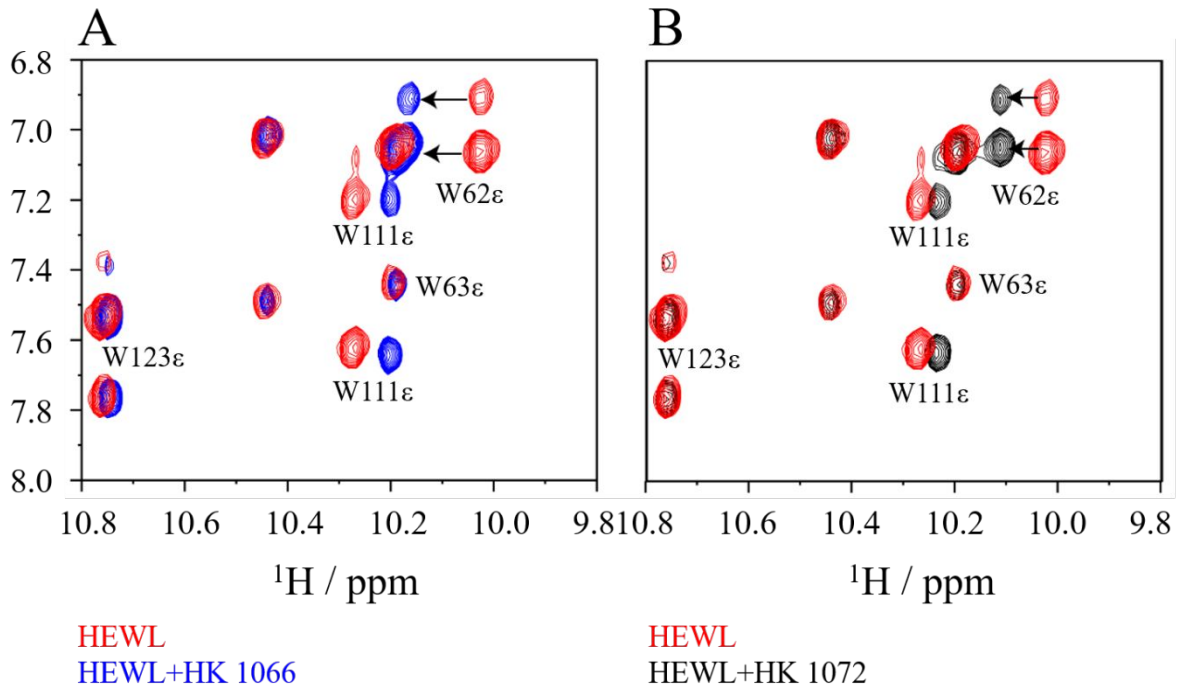

Figure 8: Chemical shift perturbation of indole (NεH) ring proton belonging to tryptophan residues of HEWL in the presence of either HK 1066 (blue) or HK 1072 (black), indicating that these moieties play a crucial role during binding of the ligand molecules.

Next, saturation transfer difference (STD) NMR was performed to define the epitope of the ligands, binding to HEWL. In this study, the ligand to HEWL concentration was kept at 300:1 ratio to enhance the „STD amplification factor"[25,26]. Careful analysis of the data suggests that both HK compounds interact with HEWL as evidenced by strong STD peaks of -CH_2/-CH_3 groups along with comparatively low signals from aromatic ring protons (Figure 9). Interestingly, the acyl chain protons (linker protons) of HK 1072 have shown comparatively stronger interaction than those associated with HK 1066 (as shown in inset), correlating well with the previous observations like ThT assays and MD simulations.

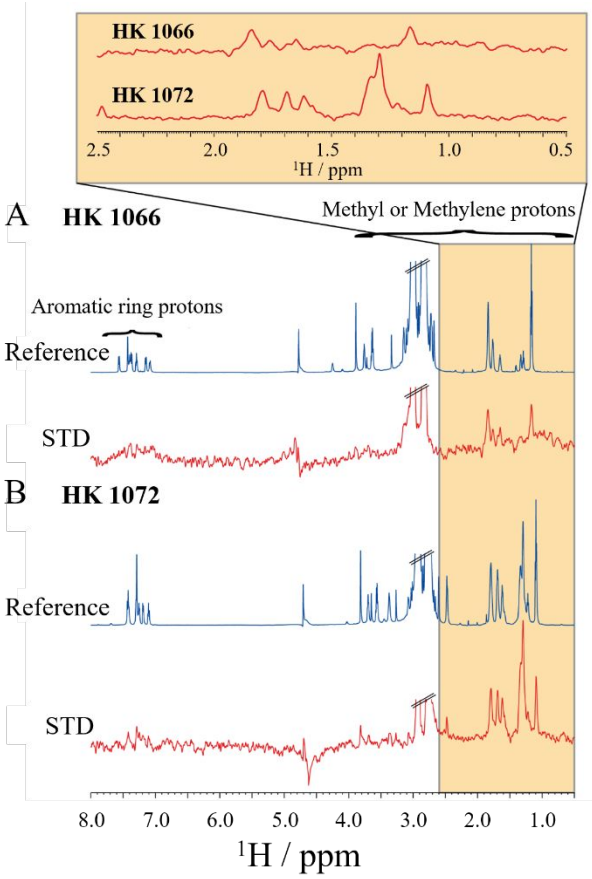

Figure 9: 1D STD NMR analysis of free and bound HK 1066 and HK 1072 in the presence of HEWL. The aliphatic (CH_2/CH_3) and aromatic ring protons of HK compounds are in close proximity to the HEWL; however, relatively stronger STD signal was observed for methylene protons of HK 1072 in comparison to HK 1066.

One of the generally accepted therapeutic strategies for amyloidoses is inhibition of amyloid aggregation of poly/peptides or/and removal of insoluble amyloid fibrils from the affected tissue. There are many reports documenting a great potential of small molecules to interfere with amyloid fibrillization of poly/peptides leading to decreasing of the amount of the amyloid aggregates. It was found that small molecules interfere with amyloid fibrillization through interaction with various amyloidogenic species produced in the aggregation process and several mechanisms of action were suggested concerning their anti-amyloid activity[7,10,29–33,12–17,27,28]. Re *et al.* suggested that intercalation of a small molecule within grooves created by β-sheets in both soluble oligomeric forms as well as in the mature amyloid fibrils leads to inhibitory activity[27]. Another proposed mode of action rests on the binding of a small molecule into the hydrophobic region of poly/peptides and interaction with neighboring amyloidogenic residues, subsequently leading to inhibition of self-assembly process and amyloid polymerization[28]. In 2014, Takai *et al.* discussed the effects of amino acids on the amyloid

aggregation of lysozyme showing that presence of cysteine significantly contributes to the inhibition of amyloid formation by non-covalent interaction between the thiol group of cysteine and the core sequence of lysozyme[29]. Ascorbic acid inhibited amyloid fibrillization of lysozyme. Proposed mechanism of action suggests binding to the aggregation-prone region of lysozyme, stabilizing its partially unfolded state, and thus preventing further conformational changes leading to fibrillization[30].

Structure-activity relationship study of several small molecules towards the amyloid aggregation of poly/peptides has been performed. It was found that presence of aromatic structures in small molecules represents important factor for anti-amyloid properties of many compounds[7,31–33]. To improve the effectivity of small compounds to influence amyloid aggregation the accumulation of cyclic structures into one multiple cyclic molecule was suggested. Lieu *et al.* demonstrated that the formation of lysozyme amyloid fibrils was markedly inhibited by the presence of rifampicin and its analogue *p*-benzoquinone, following a dose-dependent fashion[32]. Phenolic and polyphenolic compounds have been reported to inhibit the amyloid formation of poly/peptides[17]. Catechol and hydroquinone inhibited lysozyme amyloid aggregation by covalent binding to the peptide chain, forming quinoproteins[31]. A number of acridine derivatives have shown the ability to inhibit lysozyme amyloid aggregation[33]. Many other small polycyclic compounds have been tested and acknowledged as potential drug candidate prototypes for the treatment of amyloidoses[10].

Based on this knowledge, we decided to study the effect of two compounds 7-MEOTA and BTZ on the amyloid aggregation of HEWL. Both molecules consist of two (BTZ) or three (7-MEOTA) cyclic structures. Moreover, 7-MEOTA belongs to tacrine analogues for which the anti-amyloid activities have already been reported[27,34,35]. We have found that these molecules were able to affect lysozyme amyloid fibrillization to some extent. The 7-MEOTA is quite effective with IC_{50} value equal to 66.8 μM. Surprisingly, the efficiency of BTZ to inhibit HEWL fibrillization is significantly lower corresponding to IC_{50} value equal to 871.4 μM. We suggest that the reason behind this difference is lack of vdW interaction leading to lower total affinity. Overall, our data support finding that small molecules containing multiple cycles are able to interfere with amyloid aggregation.

Currently, there is a new strategy to improve the inhibitory efficiency of small compounds based on combining multiple cyclic functional molecules into one heterodimeric molecule. The aim is an enhancement of anti-aggregation capabilities due to the synergy of two or more active structures[20,22]. Besides the aromatic multicycles, a linker connecting two

functional molecules has proven to be another promising structure to optimize and modulate the effects of heterodimers. The relationship between inhibitory potency of heterodimers designed against amyloid aggregation, the structure of functional molecules and properties of the linker has been already reported in the past. In 2007, Reinke and Gestwicki defined a narrow region of optimal linker length and flexibility in case of curcumin derivatives. Both these parameters strongly influenced the potency of studied compounds against amyloid-beta aggregation[8]. In 2018, Ulicna *et al.* described a series of tacrine-coumarine heterodimers effective against amyloid aggregation of lysozyme. These derivatives differed in linker length as well as its structure. Compounds containing plain aliphatic linker have shown the greatest inhibition efficiency. It has been demonstrated that linker longer than ~ 9 Å inhibited the formation of lysozyme amyloid fibrils at lower potency, suggesting an upper limit to the effective length of linker region[28].

Our results obtained for studied heterodimers consisting of 7-MEOTA and BTZ functional molecules connected by aliphatic linker point to their significantly higher inhibitory activity compared to separate parent molecules. The IC_{50} values of studied heterodimers were lower (HK 1068 - 48.7 μM, HK 1070 - 15.4 μM, HK 1072 - 1.6 μM) than IC_{50} of functional molecules (BTZ - 871.4 μM, 7-MEOTA - 66.8 μM) with exception of derivative HK 1066 (115.6 μM). These results indicate that heterodimerization has improved the anti-amyloid properties of parent molecules. The detailed analysis of the obtained results suggests that prolonging linker increased the efficiency of heterodimers. Considering the functional molecules in heterodimers were identical, we suggest that the length of the linker region plays an important role in compounds anti-amyloid potency.

The data obtained using ThT fluorescence assay were confirmed by microscopic technique, namely by AFM. Negligible changes in amount and morphology of amyloid fibrils were observed after treatment of HEWL fibrillization with BTZ alone. Moderate inhibitory efficiency was detected for the second parent molecule 7-MEOTA as its effect was comparable with derivative with the short linker HK 1068. The effect of heterodimerization and prolonging linker was evident as changes in the amount and also morphology got more apparent in the case of heterodimers HK 1070 and HK 1072.

ATR FTIR data supported previous results since HEWL fibrillization in the presence of parent molecules BTZ and 7-MEOTA leads to subtle changes in the protein secondary structure and notable β-sheet content increase. On the other hand, the inhibitory activity of heterodimers HK 1068 and HK 1072 is represented by the extensive decrease in β-sheet content

and minor preservation of α-helical structures in produced HEWL structures compared to HEWL amyloid fibrils.

In silico methods were used to better understand the relationship between the structure of studied compounds and their inhibitory effect. Calculations indicate that the binding site of all studied compounds is very similar. Overall, the NBC network was better than HB network in the characterization of binding affinity of compounds. In all cases, compounds made NBCs with HEWL residues Asp52, Gln57, Asn59, Trp63 and Ala107. It is well established in the literature that lysozyme region 49-109 is of particular significance in the process of fibril formation. This region, including β-domain and C-helix, is considered the most amyloidogenic one of full-length HEWL[36,37]. Canet *et al.* have demonstrated the ability of β-domain and the adjacent C-helix to unfold in a locally cooperative manner[38]. Moreover, C-helix (98-109) has the lowest propensity of HEWL helices to form α-helical structure, which is likely to be a significant factor in the formation of amyloid fibrils rich in β-sheet content[37]. Although BTZ interacts with all residues mentioned above, docking study revealed it has the lowest binding affinity to HEWL. Upon further examination of NBC network for all studied compounds (Table S2) it should be noted that BTZ, in comparison to the rest of compounds including 7-MEOTA, lacks interaction with the region 44 - 48. Despite the fact that this region is not considered a major amyloidogenic contributor, interaction with this region enhances the binding affinity of small molecules to HEWL, as well as their anti-amyloid effects. Therefore, 7-MEOTA's ability to interact with these residues explains its higher affinity towards HEWL molecule and preservation of this property after the heterodimerization is possibly one of the key factors associated with the effective inhibition of HEWL amyloid aggregation by designed heterodimers.

MM-PBSA calculations support results obtained from docking study and indicate that vdW interactions predominate over electrostatic interactions in compounds binding to HEWL. To shed more light into the binding mechanism, the structure of heterodimers was divided into 3 blocks. Considering the structure of block 2 and 3 is identical for every heterodimer, their contribution to binding affinity is also identical within an error. Thus, the decisive factor that explains the variance in binding affinity of heterodimers (Table 3) and their anti-amyloid properties represented by IC_{50} values (Table 2) is block 1, the linker region (Table 4).

Regarding the lower IC_{50} value of 7-MEOTA and BTZ equimolar mixture, and also lower IC_{50} and binding affinity in comparison to 7-MEOTA alone, we believe that these are consequences of an, according to the docking simulations, identical binding sites of parent molecules. We suggest that 7-MEOTA and BTZ compete for the binding site, therefore the

efficiency is worse than individual 7-MEOTA, although not by much considering 7-MEOTA has a substantially higher affinity to HEWL. We propose a similar explanation for the compound HK 1066, which has the shortest linker among the heterodimers. 7-MEOTA (block 3) of the HK 1066 binds to its high-affinity site, while BTZ (block 2) does not and presumably competes with 7-MEOTA (block 3), which explains lower affinity compared to 7-MEOTA alone. Moreover, we observed that after heterodimerization BTZ (block 2) occupies a new binding location in close proximity to residues Phe34 and Glu35. Obtained results show a big increase in absolute binding free energy with prolonging linker region. We assume that longer linker allows BTZ (block 2) to approach the new binding site more conveniently, which is not possible especially in the case of HK 1066.

The binding free energy estimated by MM-PBSA and the number of carbon atoms in linker structure of heterodimers correlate very well (Figure 6). These subtle changes in binding free energy lead to greater stabilization of HEWL structure, preventing the creation of early amyloidogenic species. However, the sharp decline in IC_{50} values might not be the consequence of binding affinity alone. As demonstrated in docking results, studied heterodimers interact with region 49-109 considered as most important in the formation of amyloid fibrils. NBC network representation (Figure S4) and STD NMR (Figure 10) results suggest that the linker region interacts with residues in close proximity of the C-helix domain (residues 98-109). The presence of heterodimer in binding site possibly blocks the interaction between β-domain and C-helix, halting the formation of partially unordered regions essential for cross-beta structure. Prolongation of the linker ultimately enhances compounds ability to prevent this interaction by greater steric obstruction.

Conclusion

Combination of multiple functional moieties while conserving their fundamental properties into one molecule with enhanced activity is a novel approach to target amyloidoses. In this study, we investigated the activity of 7-MEOTA – BTZ heterodimers, HK compounds, towards amyloid aggregation of lysozyme. Using several *in vitro* and *in silico* techniques we showed that heterodimerization has a substantial impact on the effectivity of compounds. As a result, HK compounds exhibited a much higher ability to inhibit amyloid aggregation of HEWL in comparison to their parent molecules. Despite the fact that according to *in silico* calculations individual 7-MEOTA and BTZ molecules occupy the same binding site, the best HK compounds have more than a double binding affinity to lysozyme. In case of heterodimers we assume that BTZ (block 2), which has lower affinity than 7-MEOTA (block 3), presumably binds to another location instead of competing with 7-MEOTA. When certain conditions are met, namely the linker length, inhibitory efficacy improvement was observed. We suggest that this dependency is connected to the interaction of the aliphatic linker with residues in the C-helix sequence (98-109) of the HEWL molecule. We demonstrated that prolongation of the linker leads to the higher affinity of HK compounds as vdW interaction of linker region increases and BTZ binds more effectively. We also suggest that their anti-amyloid activity is related to the steric obstruction between β-sheet rich and C-helix regions of the HEWL molecule, which are considered essential for the formation of the amyloid structures.

The obtained results represent an important contribution for the recent rational design of potential lead small molecules with anti-amyloid properties and studied heterodimers are perspective candidates for the treatment of systemic lysozyme amyloidosis and other amyloid-related diseases.

Material and Methods

Chemicals

HEWL (L6876, activity ~40 000 units.mg^{-1} protein E.C. number: 3.2.1.17), thioflavin T (ThT), dimethyl sulfoxide (DMSO), glycine, NaCl and Dulbecco's Modified Eagle Medium (DMEM) were purchased from the Sigma Aldrich Chemicals Company (St Louis, MO). SH-SY5Y human neuroblastoma cell line was purchased from German Collection of Microorganisms and Cell Culture, DSMZ (Braunschweig, Germany) and WST-1 Cell Proliferation Assay Kit (WST-1) from Roche Diagnostics GmbH (Mannheim, Germany). 4,4-dimethyl-4-silapentane-5-sulfonate sodium salt (DSS), D_6-DMSO and D_2O were obtained from Cambridge Isotope Laboratories, Inc. (Tewksbury, MA, USA). Citrate was purchased from MERCK (MERCK Millipore, MA, USA) and disodium hydrogen phosphate was purchased from HiMedia Laboratories Pvt. Ltd, Mumbai, India. All chemicals were of analytical reagent grade. Studied 7-MEOTA – 2-aminobenzothiazole (BTZ) heterodimers (HK compounds) (Table 1) were synthesized at the Department of Chemistry, Faculty of Science, University of Hradec Kralove, Hradec Kralove, Czech Republic. All chemical reagents used for synthesis were purchased from Sigma Aldrich Chemicals Company (St Louis, MO). Solvents for synthesis were obtained from Penta chemicals (Prague, Czech Republic).

Synthesis of HK compounds

Novel 7-MEOTA-BTZ heterodimers (HK 1066, HK 1068, HK 1070 and HK 1072) were obtained as depicted in Scheme 1. 7-Methoxy-1,3,4,10-tetrahydroacridin-9(2*H*)-one, 9-chloro-7-methoxy-1,2,3,4-tetrahydroacridine as well as *N*-(7-methoxy-1,2,3,4-tetrahydroacridin-9-yl)alkanediamines were synthesized according to the procedures already reported in the literature[39,40]. Subsequent coupling with 2-chloro-1,3-benzothiazole in the presence of *N*,*N*-diisopropylethylamine (DIPEA) in dimethylformamide (DMF) at 110°C for 2 hours provided target compounds in moderate yields. All new hybrids were finally structurally characterized in the form of hydrochloride salts by their analytical and spectroscopic data.

Scheme 1. Synthesis of HK compounds (HK 1066, HK 1068, HK 1070 and HK 1072)

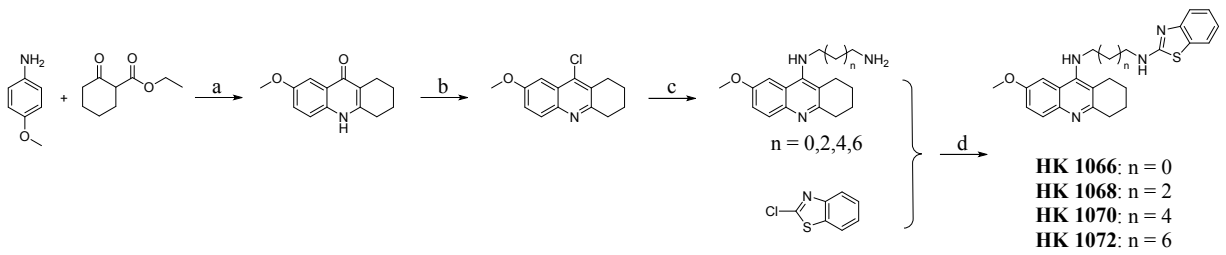

Reagents and conditions: (a) toluene, H_2O, diphenylether, EtOH, Dean-Stark trap; (b) $POCl_3$; (c) *a*,*w*-diaminoalkane, phenol; (d) DIPEA, DMF

Round-bottom flask with 2-chlorobenzothiazole (1 eq) was purged with argon and treated with DMF (5 ml). Thereafter, *N*,*N*-diisopropylethylamine (2 eq) was added to the mixture. Finally, appropriate *α*,*ω*- diaminotacrine derivative (1 eq) dissolved in a small amount of DMF was added to the flask. Formed solution was then heated to 110°C and stirred for 2 hours. After cooling to room temperature, the mixture was dissolved in CH_2Cl_2 (3 × 100 ml) and extracted with water (100 ml). Collected organic layers were dried over Na_2SO_4, filtered and evaporated to give crude product. Purification by column chromatography using ethyl acetate/MeOH/26 % aqueous ammonia solution (60/1/0.2) as eluent provided a pure base. Obtained base was dissolved in MeOH and saturated with gaseous HCl. Solvent removal afforded an oily residue which was subsequently washed with acetonitrile to give the final product in the form of hydrochloride salt.

The course of the reactions was monitored by thin-layer chromatography on aluminum plates precoated with silica gel 60 F254 (Merck, Czech Republic) and then visualized by UV 254. Melting points were determined on a melting point apparatus M-565 (Büchi, Switzerland) and are uncorrected. Uncalibrated purity was ascertained by LC-UV (at the wavelength of 254 nm) using a reverse phase C18 chromatographic column. All the biologically tested compounds exhibited purity 99 % at a wavelength 254 nm. NMR spectra of target compounds were recorded on Varian S500 spectrometer (operating at 500 MHz for ^1H and 126 MHz for ^{13}C; Varian Comp. Palo Alto, USA). Chemical shifts are reported in parts per million (ppm). Spin multiplicities are given as s (singlet), d (doublet), dd (doublet of doublets), t (triplet), p (pentaplet), or m (multiplet). The coupling constants (*J*) are reported in Hertz (Hz). High-resolution mass spectra (HRMS) were determined by Q Exactive Plus hybrid quadrupole-orbitrap spectrometer.

N^2-(1,3-benzothiazol-2-yl)-N^1-(7-methoxy-1,2,3,4-tetrahydroacridin-9-yl)ethane-1,2-diamine hydrochloride (HK 1066)

Yield 38 %. mp 190.4 – 191.6°C. Purity: 99 %. ^{1}H NMR (500 MHz, Methanol-d_4) δ 7.73 (d, J = 8.0 Hz, 1H), 7.68 (d, J = 2.6 Hz, 1H), 7.62 (d, J = 9.2 Hz, 1H), 7.51 – 7.44 (m, 2H), 7.37 – 7.32 (m, 2H), 4.31 (t, J = 5.7 Hz, 2H), 4.00 (t, J = 5.7 Hz, 2H), 3.96 (s, 3H), 3.05 (t, J = 6.3 Hz, 2H), 2.86 (t, J = 6.2 Hz, 2H), 2.00 – 1.89 (m, 4H). ^{13}C NMR (126 MHz, DMSO-d_6) δ 167.01, 163.15, 156.84, 155.33, 150.34, 132.48, 126.79, 124.05, 123.22, 122.31, 120.84, 118.06, 112.37, 103.43, 56.36, 45.55, 28.04, 25.43, 24.81, 21.89, 20.28. HRMS: $[M+H]^+$ 405.1742 (calculated for $[C_{23}H_{25}N_4OS]^+$: 405.1704).

N^4-(1,3-benzothiazol-2-yl)-N^1-(7-methoxy-1,2,3,4-tetrahydroacridin-9-yl)butane-1,4-diamine hydrochloride (HK 1068)

Yield 16 %. mp 174.9 – 175.1°C. Purity: 99 %. ^{1}H NMR (500 MHz, Methanol-d_4) δ 7.79 (d, J = 7.9 Hz, 1H), 7.70 – 7.63 (m, 2H), 7.58 – 7.48 (m, 2H), 7.45 – 7.35 (m, 2H), 4.02 (t, J = 6.5 Hz, 2H), 3.96 (s, 3H), 3.70 – 3.61 (m, 2H), 3.00 (t, J = 5.4 Hz, 2H), 2.79 (t, J = 5.3 Hz, 2H), 2.04 – 1.85 (m, 8H). ^{13}C NMR (126 MHz, Methanol-d_4) δ 158.74, 157.04, 151.00, 139.40, 134.19, 129.18, 126.29, 125.40, 124.43, 123.92, 121.71, 118.90, 115.20, 113.25, 104.61, 56.77, 47.78, 29.30, 28.99, 26.31, 26.02, 23.18, 21.79. HRMS: $[M+H]^+$ 433.2056 (calculated for $[C_{25}H_{29}N_4OS]^+$: 433.2017).

N^6-(1,3-benzothiazol-2-yl)-N^1-(7-methoxy-1,2,3,4-tetrahydroacridin-9-yl)hexane-1,6-diamine hydrochloride (HK 1070)

Yield 27 %. mp 151.7 – 152.6°C. Purity: 99 %. ^{1}H NMR (500 MHz, Methanol-d_4) δ 7.81 (d, J = 8.0 Hz, 1H), 7.73 (d, J = 9.3 Hz, 1H), 7.69 (d, J = 2.6 Hz, 1H), 7.58 (dd, J = 8.1, 1.1 Hz, 1H), 7.55 – 7.49 (m, 2H), 7.41 – 7.36 (m, 1H), 3.99 – 3.94 (m, 5H), 3.58 (t, J = 7.0 Hz, 2H), 3.04 – 2.99 (m, 2H), 2.77 (t, J = 5.8 Hz, 2H), 1.95 (p, J = 3.1 Hz, 4H), 1.92 – 1.85 (m, 2H), 1.85 – 1.78 (m, 2H), 1.61 – 1.50 (m, 4H). ^{13}C NMR (126 MHz, Methanol-d_4) δ 158.65, 157.20, 150.74, 139.48, 134.48, 129.23, 126.29, 125.40, 123.92, 121.75, 118.69, 115.15, 112.92, 105.02, 56.62, 48.52, 31.81, 29.25, 29.14, 27.42, 27.33, 25.66, 23.17, 21.86. HRMS: $[M+H]^+$ 461.2366 (calculated for $[C_{27}H_{33}N_4OS]^+$: 461.2330).

N^8-(1,3-benzothiazol-2-yl)-N^1-(7-methoxy-1,2,3,4-tetrahydroacridin-9-yl)octane-1,8-diamine hydrochloride (HK 1072)

Yield 15 %. mp 146.8 – 147.4°C. Purity: 99 %. ^{1}H NMR (500 MHz, Methanol-d_4) δ 7.78 (d, J = 7.8 Hz, 1H), 7.74 (d, J = 9.2 Hz, 1H), 7.65 (d, J = 2.5 Hz, 1H), 7.60 – 7.54 (m, 1H), 7.52 – 7.44 (m, 2H), 7.38 – 7.31 (m, 1H), 3.96 (s, 3H), 3.95 – 3.88 (m, 2H), 3.57 (t, J = 7.1 Hz, 2H), 3.06 – 2.98 (m, 2H), 2.79 – 2.70 (m, 2H), 1.99 – 1.90 (m, 4H), 1.88 – 1.74 (m, 4H), 1.55 – 1.36 (m, 8H). ^{13}C NMR (126 MHz, Methanol-d_4) δ 158.50, 157.04, 150.57, 139.82, 134.39, 129.05, 126.07, 125.33, 124.59, 123.81, 121.73, 118.54, 115.24, 112.76, 104.93, 56.65, 48.59, 31.95, 30.15, 30.07, 29.22, 27.66, 27.63, 25.62, 23.14, 21.84. HRMS: $[M+H]^+$ 489.2682 (calculated for $[C_{29}H_{37}N_4OS]^+$: 489.2683).

In vitro lysozyme amyloid aggregation – ThT fluorescence assay

HEWL was dissolved in 70 mM glycine buffer with an addition of 80 mM NaCl at pH 2.7 to a final concentration of 10 μM. The HEWL solution was incubated at 65°C for 2 h and stirred at 1200 rpm in thermomixer. After the incubation, the amyloid-specific dye ThT was added and samples were incubated for another 60 min at 37°C in dark. The formation of HEWL amyloid fibrils was confirmed by a significant increase in ThT fluorescence. Measurements were performed in a 96-well plate using a Synergy MX (BioTek) spectrofluorimeter. The excitation wavelength was set at 440 nm and the emission recorded at 485 nm. The excitation and emission slits were adjusted to 9.0/9.0 nm and the top probe vertical offset was 6 mm.

Effect of compounds on HEWL amyloid fibrillization; determination of IC_{50} values.

Interference of BTZ, 7-MEOTA and HK compounds with an amyloid aggregation of HEWL was studied using ThT fluorescence assay in the concentration range of 100 pM to 1 mM at fixed 10 μM protein concentration. All compounds were dissolved in DMSO. To clarify the possible binding competition between ThT and studied compounds, we underwent an additional experiment detailly described in the SI (*Control experiment - clarification of the potential competitive binding among ThT and studied compounds, Figure S10*). Recorded ThT fluorescence intensities were normalized to the ThT fluorescence of lysozyme amyloid fibrils in the absence of studied compounds.

Atomic force microscopy (AFM)

Samples for AFM were applied on the freshly cleaved mica. After 5 min adsorption the surface of mica was rinsed several times with ultrapure water and left to dry. AFM images were obtained using a Scanning Probe Microscope (Veeco di Innova) in a tapping mode using NCHV cantilever with a specific resistance 0.01 – 0.025 $\Omega.cm^{-1}$. All images are unfiltered.

Attenuated total reflectance Fourier transform infrared (ATR-FTIR) spectroscopy

Attenuated total reflectance FTIR (ATR-FTIR) spectra were recorded using Nicolet™ 8700 Fourier transform infrared spectrometer (Thermo Fisher Scientific) equipped with Smart OMNI-Sampler (diamond crystal). A quantity of 5 µl of a sample (50 µM HEWL, 500 µM compound) was spread on the diamond surface. Each spectrum represents an average of 254 repetitions, recorded at the resolution of 2 cm^{-1} in amide I region (1700 – 1600 cm^{-1}). Recorded spectra were smoothed using OMNIC 8 software (Thermo Fisher Scientific) to achieve the quality of spectra adequate for deconvolution. 11-point Savitzky–Golay filter (10.607 cm^{-1}) followed by 7-point Savitzky–Golay filter (6.750 cm^{-1}) was applied. Spectra were subsequently deconvoluted by peak analyzer in OriginPro 8 (OriginLab Corporation). Baseline was substracted and the positions of peaks in amide I region were added manually in correlation with raw data. To assign peak positions to the secondary structures, measurements were compared against the published literature[41]. Gaussian peak function was used to fit the data and particular secondary structures content was obtained by gaussian curves area integration.

Statistical analysis

All experiments were performed at least in triplicate and the presented data are expressed as the mean value with average deviation of n independent measurements ($n \geq 3$). Specific n value are now reported in the figure legends. IC_{50} values (compound concentration with 50 % inhibitory activity) were determined from curves obtained by fitting the average values with non-linear least-square method (Sigmoid, Parameter 3 in the SigmaPlot software (Systat Software Inc., USA)) using equation: $y + a/(1 + \exp(+(x - x_0)/b))$, where x_0 corresponds to IC_{50} value. The FTIR spectra of amide I region (1700 – 1600 cm^{-1}) represent an average of 254 repetitions. The content of the secondary structures was obtained by deconvolution of the spectra using peak analyser in OriginPro 8 (OriginLab Corporation), namely the Gaussian peak function allowing determination of the particular secondary structure content (%) by Gaussian

curves area integration. The precision of deconvolution fit is given by correlation coefficient adjusted R^2 in Table S1.

Receptor and ligands – in silico methods

The structure of HEWL monomer was taken from Protein Data Bank with PDB ID 193L[42] at pH 4.3. Then, using PDB2PQR[43] server with Amber force field and PROPKA[44,45], the pH calculation was performed to decrease pH to 2.7 and the obtained structure is shown in Figure 10A. There are 4 disulfide bonds between residues C6 - C127, C30 - C115, C64 - C80, and C76 - C94 in this structure, therefore 4 S-S bonds were added into the simulation to preserve these bonds.

Marvin Sketch 17.24 was used to get 3D structures of HK compounds at pH 2.7 (Figure 10B), at which IC_{50} values have been experimentally determined. The structures of six compounds including 7-MEOTA, BTZ, HK 1066, HK 1068, HK 1070 and HK 1072 were optimized using Gaussian 09 software[46] at the B3LYP/6-31G(d) level of theory.

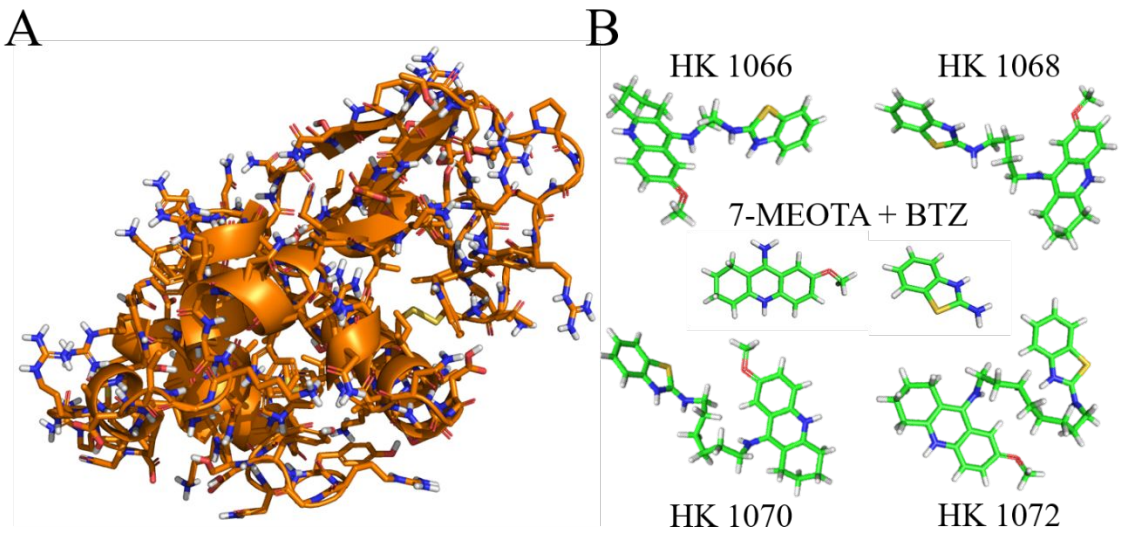

Figure 10. The 3D structures of studied receptor protein and compounds at pH 2.7. (A) The structure of HEWL. The sidechain hydrogen and nitrogen atoms are colored in white and blue, respectively; disulfide bonds are colored in yellow. (B) The structures of parent molecules 7-MEOTA, BTZ and synthesized heterodimers HK 1066, HK 1068, HK 1070 and HK 1072.

Docking method

AutoDock Tools 1.5.4[47] was used to prepare the input for docking simulation with PDBQT format. Then, six compounds were docked to the receptor by using AutoDock Vina 1.2[48]. For global search, the exhaustiveness value was set to 800 to get reliable results. Ten modes of flexible ligand were generated, and the receptor dynamics was neglected. The lowest binding energy in the best docking mode was selected as the scoring function for the binding affinity.

Molecular dynamics simulation

Molecular dynamics (MD) simulation was performed using GROMACS 2019[49,50]. The receptor-ligand structure obtained in the best docking mode was utilized as input for MD simulation with the AMBER99SB-ILN force field[51]. Parameters of ligand that characterize bond, angle, dihedral, improper and non-bonded interactions were computed using Antechamber[52] and Acpype[53] based on the General Amber Force Field (GAFF)[54]. Atomic point charges were determined by AM1-BCC[55].

The protein-ligand complexes were solvated in a cubic box by water molecules using the TIP3P model[56]. Then, counterions were added to neutralize the system. After that, a concentration of 70 mM glycine and 80 mM NaCl was added to simulate the experimental conditions. The leap-frog algorithm[57] was used to integrate equations of motion with a time step of 2 fs. The LINCS algorithm was utilized to constrain bonds[58]. Systems were minimized using the steepest descent algorithm. Then, they were equilibrated in NVT for 500 ps and NPT for 5 ns ensembles at 298 K and 1 atm. The temperature and pressure were maintained by the v-rescale thermostat[59] and Parrinello-Rahman barostat[60]. A cutoff of 1.2 nm was used to estimate the van der Waals (vdW) force, while the long-range electrostatic interaction was calculated using the PME (particle mesh Ewald) method[61]. A 100 ns MD simulation was performed, and the snapshots were recorded every 10 ps at equilibrium.

MM-PBSA method

In the MM-PBSA method[62], which was presented in more detail in previous studies[63–65], the binding free energy of ligand to the receptor is given by the following equation,

$$\Delta G_{bind} = \Delta E_{elec} + \Delta E_{vdw} + \Delta G_{SA} + \Delta G_{PB} - T\Delta S, \qquad (1)$$

where ΔE_{elec}, ΔE_{vdw}, ΔG_{sur}, and ΔG_{GB} are the electrostatic, vdW, non-polar and polar solvation energies, respectively. The electrostatic and vdW interaction energy was calculated using the same parameters as in the MD simulation. The non-polar solvation energy was obtained by the formula $\Delta G_{SA} = \gamma SASA$, where SASA stands for solvate accessible surface area (Å^2), calculated from the SASA tool in the GROMACS package and $\gamma = 0.0072$ kcal.mol^{-1}Å^{-2} [66]. The polar solvation energy was calculated using the APBS package[67]. The entropy contribution, $-T\Delta S$ was obtained using the method proposed by Duan *et al*[68].

Tools and measures used for data analysis

RMSD (root mean square deviation) was calculated as the deviation of the C-alpha atoms of the receptor from the initial structure. A hydrogen bond (HB) was formed if the distance between donor D and acceptor A is < 3.5 Å, the H-A distance < 2.7 Å and the D-H-A angle > 135 degrees. A non-bonded contact (NBC) is a non-covalent bonded contact other than HB. It is defined as the contact between the C or S atom of a ligand and any atom of a protein or water molecule when they are at a distance of 2.9 - 3.9 Å. The HBs and NBCs were analyzed using LigPlot++ version 1.44[69].

Nuclear magnetic resonance

All NMR experiments were done at 25°C either on a Bruker Avance III 500 MHz equipped with a 5 mm SMART probe or 700 MHz NMR spectrometer equipped with a RT probe. HEWL samples (500 μM) were prepared by using 10 mM citrate-phosphate buffer with 100 mM NaCl (pH - 2.8) and 10 % D_2O was added for locking purpose. DSS was used as an internal standard (0.00 ppm). HK 1066 and HK 1072 were first dissolved in D6-DMSO and then diluted into the same buffer for all the experiments. Two-dimensional (^{1}H) total correlation spectroscopy (2D TOCSY), and Nuclear Overhauser Spectroscopy (2D NOESY) was recorded for HEWL in free and bound (1:1 HEWL and ligand) form with a mixing time of 80 ms and 150 ms, respectively and the spectral width was set to 15 ppm in both directions. One dimensional STD NMR was performed using 1 mM concentration of ligand molecules.

The chemical shifts of the HEWL from 2D 1H-1H TOCSY (mixing time 80 ms) and NOESY (mixing time 150 ms) experiments were assesed and compared with the reference chemical shift[70], deposited in BMRB. The identity of the chemical shifts of the HEWL residues interacting with HK compounds obtained from MD simulation study has been also subsequently cross validated.

STD NMR spectra were acquired at a ligand/HEWL mixture ratio of 300:1. Selective irradiation of HEWL was achieved by a train of Gaussian-shaped pulses with a 1 % truncation and each of 49 ms in duration and separated by a 1 ms delay. A total of 40 selected pulses were applied, leading to a total time of saturation of 2 s. The so-called on resonance for HEWL was fixed at 0.2 ppm, and off-resonance was at 40 ppm, where neither protein nor the ligand resonances were present. Subtraction of the two spectra (on-resonance – off-resonance) by phase cycling leads to the difference spectrum that contains signals arising from the saturation transfer. The reference spectrum was recorded with 640 scans, while the difference spectrum was obtained with 1280 scans. Data processing was performed using TOPSPIN program suite for all the spectra and peak assignment was done using SPARKY software.

Acknowledgement

This work was supported by the research grant projects in frame of VEGA 2/0145/17, MVTS COST 083/14 action BM1405, APVV-18-0284, the project Excellence of the University of Hradec Kralove, Polish NCN grant 2015/19/B/ST4/02721, Poland, project B2019.SPD.03 and Department of Science and Technology, Ho Chi Minh city, Vietnam. This research was partially supported in by PLGrid Infrastructure, Poland.

Author Contributions

M. G. and K. H. contributed equally. M. S. L. and Z.G. conceived the experiments. Z. G., Z. B. and M. G. designed *in vitro* experiments and analyzed results, M. G. and Z. B. performed *in vitro* experiments. M. S. L. designed *in silico* experiments, K. H., N. Q. T. and H. L. N. performed *in silico* experiments. S. A. M. and A. B. designed and performed NMR experiments and analyzed the data. E. N. synthesized the HK compounds. Z. G. and M. G. wrote the paper. All authors reviewed the manuscript.

Supporting Information

- FTIR peak analysis, deconvolution and secondary structure percentage distributions

- list of residues forming non-bonded contacts with HK compounds

- 3D images of docking poses and contact networks of studied compounds

- correlations between docking binding energy, binding free energy (MM-PBSA), IC50 values, ΔG_{exp} and time dependence of Cα RMSD of lysozyme bound to studied molecules

- control experiment - clarification of the potential competitive binding among ThT and studied compounds

References

(1) Dobson, C. M. Protein Folding and Misfolding. *Nature* **2003**, *426* (6968), 884–890.

(2) Abbaskhani, Z. Effect of Metal Ions on Aggregation of Amyloid Beta Peptide. *Parkinsonism Relat. Disord.* **2016**, *22*, e191–e192.

(3) Khlistunova, I.; Biernat, J.; Wang, Y.; Pickhardt, M.; von Bergen, M.; Gazova, Z.; Mandelkow, E.; Mandelkow, E.-M. Inducible Expression of Tau Repeat Domain in Cell Models of Tauopathy. *J. Biol. Chem.* **2006**, *281* (2), 1205–1214.

(4) Sattianayagam, P. T.; Gibbs, S. D. J.; Rowczenio, D.; Pinney, J. H.; Wechalekar, A. D.; Gilbertson, J. A.; Hawkins, P. N.; Lachmann, H. J.; Gillmore, J. D. Hereditary Lysozyme Amyloidosis - Phenotypic Heterogeneity and the Role of Solid Organ Transplantation. *J. Intern. Med.* **2012**, *272* (1), 36–44.

(5) Wang, S.; Kestler, D.; Coriu, D.; Solomon, A.; Murphy, C.; Wooliver, C.; Weiss, D. Familial Amyloidosis Associated with a Novel Mutation (D68g) in the Lysozyme Gene. In *XIth International Symposium on Amyloidosis*; CRC Press, 2007; pp 208–210.

(6) Mocanu, M.-M.; Ganea, C.; Siposova, K.; Filippi, A.; Demjen, E.; Marek, J.; Bednarikova, Z.; Antosova, A.; Baran, I.; Gazova, Z. Polymorphism of Hen Egg White Lysozyme Amyloid Fibrils Influences the Cytotoxicity in LLC-PK1 Epithelial Kidney Cells. *Int. J. Biol. Macromol.* **2014**, *65*, 176–187.

(7) Ramazzotti, M.; Melani, F.; Marchi, L.; Mulinacci, N.; Gestri, S.; Tiribilli, B.; Degl'Innocenti, D. Mechanisms for the Inhibition of Amyloid Aggregation by Small Ligands. *Biosci. Rep.* **2016**, *36* (5), e00385–e00385.

(8) Reinke, A. A.; Gestwicki, J. E. Structure?Activity Relationships of Amyloid Beta-Aggregation Inhibitors Based on Curcumin: Influence of Linker Length and Flexibility. *Chem. Biol. Drug Des.* **2007**, *70* (3), 206–215.

(9) Simone Tranches Dias, K.; Viegas, C. Multi-Target Directed Drugs: A Modern Approach for Design of New Drugs for the Treatment of Alzheimer's Disease. *Curr. Neuropharmacol.* **2014**, *12* (3), 239–255.

(10) de Freitas Silva, M.; Dias, K. S. T.; Gontijo, V. S.; Ortiz, C. J. C.; Viegas, C. Multi-Target Directed Drugs as a Modern Approach for Drug Design Towards Alzheimer's Disease: An Update. *Curr. Med. Chem.* **2018**, *25* (29), 3491–3525.

(11) Orteca, G.; Tavanti, F.; Bednarikova, Z.; Gazova, Z.; Rigillo, G.; Imbriano, C.; Basile, V.; Asti, M.; Rigamonti, L.; Saladini, M.; et al. Curcumin Derivatives and Aβ-Fibrillar Aggregates: An Interactions' Study for Diagnostic/Therapeutic Purposes in Neurodegenerative Diseases. *Bioorg. Med. Chem.* **2018**, *26* (14), 4288–4300.

(12) Doig, A. J.; Derreumaux, P. Inhibition of Protein Aggregation and Amyloid Formation by Small Molecules. *Curr. Opin. Struct. Biol.* **2015**, *30*, 50–56.

(13) Shuaib, S.; Goyal, B. Scrutiny of the Mechanism of Small Molecule Inhibitor Preventing Conformational Transition of Amyloid-β 42 Monomer: Insights from Molecular Dynamics Simulations. *J. Biomol. Struct. Dyn.* **2018**, *36* (3), 663–678.

(14) Van Vuong, Q.; Bednarikova, Z.; Antosova, A.; Huy, P. D. Q.; Siposova, K.; Tuan, N. A.; Li, M. S.; Gazova, Z. Inhibition of Insulin Amyloid Fibrillization by Glyco-Acridines: An in Vitro and in Silico Study. *Medchemcomm* **2015**, *6* (5), 810–822.

(15) Vuong, Q. Van; Siposova, K.; Nguyen, T. T.; Antosova, A.; Balogova, L.; Drajna, L.; Imrich, J.; Li, M. S.; Gazova, Z. Binding of Glyco-Acridine Derivatives to Lysozyme Leads to Inhibition of Amyloid Fibrillization. *Biomacromolecules* **2013**, *14* (4), 1035–1043.

(16) Siddiqi, M. K.; Alam, P.; Chaturvedi, S. K.; Khan, M. V.; Nusrat, S.; Malik, S.; Khan, R. H. Capreomycin Inhibits the Initiation of Amyloid Fibrillation and Suppresses Amyloid Induced Cell Toxicity. *Biochim. Biophys. Acta, Proteins Proteomics* **2018**, *1866* (4), 549–557.

(17) Gazova, Z.; Siposova, K.; Kurin, E.; Mučaji, P.; Nagy, M. Amyloid Aggregation of Lysozyme: The Synergy Study of Red Wine Polyphenols. *Proteins: Struct., Funct., Bioinf.* **2013**, *81* (6), 994–1004.

(18) Summers, W. K. Tacrine, and Alzheimer's Treatments*. *J. Alzheimer's Dis.* **2006**, *9*

(s3), 439–445.

(19) Korabecny, J.; Musilek, K.; Holas, O.; Binder, J.; Zemek, F.; Marek, J.; Pohanka, M.; Opletalova, V.; Dohnal, V.; Kuca, K. Synthesis and in Vitro Evaluation of N-Alkyl-7-Methoxytacrine Hydrochlorides as Potential Cholinesterase Inhibitors in Alzheimer Disease. *Bioorg. Med. Chem. Lett.* **2010**, *20* (20), 6093–6095.

(20) Gazova, Z.; Soukup, O.; Sepsova, V.; Siposova, K.; Drtinova, L.; Jost, P.; Spilovska, K.; Korabecny, J.; Nepovimova, E.; Fedunova, D.; et al. Multi-Target-Directed Therapeutic Potential of 7-Methoxytacrine-Adamantylamine Heterodimers in the Alzheimer's Disease Treatment. *Biochim. Biophys. Acta, Mol. Basis Dis.* **2017**, *1863* (2), 607–619.

(21) Keri, R. S.; Patil, M. R.; Patil, S. A.; Budagumpi, S. A Comprehensive Review in Current Developments of Benzothiazole-Based Molecules in Medicinal Chemistry. *Eur. J. Med. Chem.* **2015**, *89*, 207–251.

(22) Thai, N. Q.; Bednarikova, Z.; Gancar, M.; Linh, H. Q.; Hu, C.-K.; Li, M. S.; Gazova, Z. Compound CID 9998128 Is a Potential Multitarget Drug for Alzheimer's Disease. *ACS Chem. Neurosci.* **2018**, *9* (11), 2588–2598.

(23) Kabsch, W.; Sander, C. Dictionary of Protein Secondary Structure: Pattern Recognition of Hydrogen-Bonded and Geometrical Features. *Biopolymers* **1983**, *22* (12), 2577–2637.

(24) Tu, L.-H.; Raleigh, D. P. Role of Aromatic Interactions in Amyloid Formation by Islet Amyloid Polypeptide. *Biochemistry* **2013**, *52* (2), 333–342.

(25) Mayer, M.; Meyer, B. Group Epitope Mapping by Saturation Transfer Difference NMR To Identify Segments of a Ligand in Direct Contact with a Protein Receptor. *J. Am. Chem. Soc.* **2001**, *123* (25), 6108–6117.

(26) Bhunia, A.; Bhattacharjya, S.; Chatterjee, S. Applications of Saturation Transfer Difference NMR in Biological Systems. *Drug Discovery Today* **2012**, *17* (9–10), 505–513.

(27) Takai, E.; Uda, K.; Matsushita, S.; Shikiya, Y.; Yamada, Y.; Shiraki, K.; Zako, T.; Maeda, M. Cysteine Inhibits Amyloid Fibrillation of Lysozyme and Directs the Formation of Small Worm-like Aggregates through Non-Covalent Interactions. *Biotechnol. Prog.* **2014**, *30* (2), 470–478.

(28) Patel, P.; Parmar, K.; Patel, D.; Kumar, S.; Trivedi, M.; Das, M. Inhibition of Amyloid Fibril Formation of Lysozyme by Ascorbic Acid and a Probable Mechanism of Action. *Int. J. Biol. Macromol.* **2018**, *114*, 666–678.

(29) Feng, S.; Song, X.-H.; Zeng, C.-M. Inhibition of Amyloid Fibrillation of Lysozyme by Phenolic Compounds Involves Quinoprotein Formation. *FEBS Lett.* **2012**, *586* (22), 3951–3955.

(30) Lieu, V. H.; Wu, J. W.; Wang, S. S.-S.; Wu, C.-H. Inhibition of Amyloid Fibrillization of Hen Egg-White Lysozymes by Rifampicin and p-Benzoquinone. *Biotechnol. Prog.* **2008**, *23* (3), 698–706.

(31) Gazova, Z.; Bellova, A.; Daxnerova, Z.; Imrich, J.; Kristian, P.; Tomascikova, J.; Bagelova, J.; Fedunova, D.; Antalik, M. Acridine Derivatives Inhibit Lysozyme Aggregation. *Eur. Biophys. J.* **2008**, *37* (7), 1261–1270.

(32) Re, F.; Airoldi, C.; Zona, C.; Masserini, M.; Ferla, B. La; Quattrocchi, N.; Nicotra, F. Beta Amyloid Aggregation Inhibitors: Small Molecules as Candidate Drugs for Therapy of Alzheimers Disease. *Curr. Med. Chem.* **2010**, *17* (27), 2990–3006.

(33) Ulicna, K.; Bednarikova, Z.; Hsu, W.-T.; Holztragerova, M.; Wu, J. W.; Hamulakova, S.; Wang, S. S. S.; Gazova, Z. Lysozyme Amyloid Fibrillization in Presence of Tacrine/Acridone-Coumarin Heterodimers. *Colloids Surf., B* **2018**, *166*, 108–118.

(34) Romero, A.; Cacabelos, R.; Oset-Gasque, M. J.; Samadi, A.; Marco-Contelles, J. Novel Tacrine-Related Drugs as Potential Candidates for the Treatment of Alzheimer's Disease. *Bioorg. Med. Chem. Lett.* **2013**, *23* (7), 1916–1922.

(35) Nepovimova, E.; Uliassi, E.; Korabecny, J.; Peña-Altamira, L. E.; Samez, S.; Pesaresi, A.; Garcia, G. E.; Bartolini, M.; Andrisano, V.; Bergamini, C.; et al. Multitarget Drug Design Strategy: Quinone–Tacrine Hybrids Designed To Block Amyloid-β Aggregation and To Exert Anticholinesterase and Antioxidant Effects. *J. Med. Chem.* **2014**, *57* (20), 8576–8589.

(36) Frare, E.; Polverino de Laureto, P.; Zurdo, J.; Dobson, C. M.; Fontana, A. A Highly Amyloidogenic Region of Hen Lysozyme. *J. Mol. Biol.* **2004**, *340* (5), 1153–1165.

(37) Krebs, M. R. H.; Wilkins, D. K.; Chung, E. W.; Pitkeathly, M. C.; Chamberlain, A. K.; Zurdo, J.; Robinson, C. V.; Dobson, C. M. Formation and Seeding of Amyloid Fibrils from Wild-Type Hen Lysozyme and a Peptide Fragment from the β-Domain. *J. Mol. Biol.* **2000**, *300* (3), 541–549.

(38) Canet, D.; Last, A. M.; Tito, P.; Sunde, M.; Spencer, A.; Archer, D. B.; Redfield, C.; Robinson, C. V.; Dobson, C. M. Local Cooperativity in the Unfolding of an Amyloidogenic Variant of Human Lysozyme. *Nat. Struct. Biol.* **2002**, *9* (4), 308–315.

(39) Korabecny, J.; Dolezal, R.; Cabelova, P.; Horova, A.; Hruba, E.; Ricny, J.; Sedlacek, L.; Nepovimova, E.; Spilovska, K.; Andrs, M.; et al. 7-MEOTA-Donepezil like Compounds as Cholinesterase Inhibitors: Synthesis, Pharmacological Evaluation, Molecular Modeling and QSAR Studies. *Eur. J. Med. Chem.* **2014**, *82*, 426–438.

(40) Spilovska, K.; Korabecny, J.; Kral, J.; Horova, A.; Musilek, K.; Soukup, O.; Drtinova, L.; Gazova, Z.; Siposova, K.; Kuca, K. 7-Methoxytacrine-Adamantylamine Heterodimers as Cholinesterase Inhibitors in Alzheimer's Disease Treatment - Synthesis, Biological Evaluation and Molecular Modeling Studies. *Molecules* **2013**, *18* (2), 2397–2418.

(41) Yang, H.; Yang, S.; Kong, J.; Dong, A.; Yu, S. Obtaining Information about Protein Secondary Structures in Aqueous Solution Using Fourier Transform IR Spectroscopy. *Nat. Protoc.* **2015**, *10* (3), 382–396.

(42) Vaney, M. C.; Maignan, S.; Riès-Kautt, M.; Ducruix, A. High-Resolution Structure (1.33 Å) of a HEW Lysozyme Tetragonal Crystal Grown in the APCF Apparatus. Data and Structural Comparison with a Crystal Grown under Microgravity from SpaceHab-01 Mission. *Acta Crystallogr., Sect. D: Biol. Crystallogr.* **1996**, *52* (3), 505–517.

(43) Dolinsky, T. J.; Nielsen, J. E.; McCammon, J. A.; Baker, N. A. PDB2PQR: An Automated Pipeline for the Setup of Poisson-Boltzmann Electrostatics Calculations. *Nucleic Acids Res.* **2004**, *32* (1), W665–W667.

(44) Søndergaard, C. R.; Olsson, M. H. M.; Rostkowski, M.; Jensen, J. H. Improved

Treatment of Ligands and Coupling Effects in Empirical Calculation and Rationalization of p K a Values. *J. Chem. Theory Comput.* **2011**, *7* (7), 2284–2295.

(45) Olsson, M. H. M.; Søndergaard, C. R.; Rostkowski, M.; Jensen, J. H. PROPKA3: Consistent Treatment of Internal and Surface Residues in Empirical p K a Predictions. *J. Chem. Theory Comput.* **2011**, *7* (2), 525–537.

(46) Frisch, M. J.; Trucks, G. W.; Schlegel, H. B.; Scuseria, G. E.; Robb, M. A.; Cheeseman, J. R.; Scalmani, G.; Barone, V.; Mennucci, B.; Petersson, G. A.; et al. Gaussian 09, Revision B.01. *Gaussian 09, Revis. B.01, Gaussian, Inc., Wallingford CT* **2009**, *29* (5), 839–845.

(47) Sanner, M. F. Python: A Programming Language for Software Integration and Development. *J. Mol. Graph. Model.* **1999**, *17* (1), 57–61.

(48) Trott, O.; Olson, A. J. AutoDock Vina: Improving the Speed and Accuracy of Docking with a New Scoring Function, Efficient Optimization, and Multithreading. *J. Comput. Chem.* **2009**, *31* (2), 455–461.

(49) Abraham, M. J.; Murtola, T.; Schulz, R.; Páll, S.; Smith, J. C.; Hess, B.; Lindahl, E. GROMACS: High Performance Molecular Simulations through Multi-Level Parallelism from Laptops to Supercomputers. *SoftwareX* **2015**, *1–2*, 19–25.

(50) Berendsen, H. J. C.; van der Spoel, D.; van Drunen, R. GROMACS: A Message-Passing Parallel Molecular Dynamics Implementation. *Comput. Phys. Commun.* **1995**, *91* (1–3), 43–56.

(51) Hornak, V.; Abel, R.; Okur, A.; Strockbine, B.; Roitberg, A.; Simmerling, C. Comparison of Multiple Amber Force Fields and Development of Improved Protein Backbone Parameters. *Proteins: Struct., Funct., Bioinf.* **2006**, *65* (3), 712–725.

(52) Wang, J.; Wang, W.; Kollman, P. a; Case, D. a. Antechamber, An Accessory Software Package For Molecular Mechanical Calculations. *J. Am. Chem. Soc* **2001**, *222*, U403.

(53) Sousa da Silva, A. W.; Vranken, W. F. ACPYPE - AnteChamber PYthon Parser InterfacE. *BMC Res. Notes* **2012**, *5* (1), 367.

(54) Wang, J.; Wolf, R. M.; Caldwell, J. W.; Kollman, P. A.; Case, D. A. Development and Testing of a General Amber Force Field. *J. Comput. Chem.* **2004**, *25* (9), 1157–1174.

(55) Jakalian, A.; Jack, D. B.; Bayly, C. I. Fast, Efficient Generation of High-Quality Atomic Charges. AM1-BCC Model: II. Parameterization and Validation. *J. Comput. Chem.* **2002**, *23* (16), 1623–1641.

(56) Jorgensen, W. L.; Chandrasekhar, J.; Madura, J. D.; Impey, R. W.; Klein, M. L. Comparison of Simple Potential Functions for Simulating Liquid Water. *J. Chem. Phys.* **1983**, *79* (2), 926–935.

(57) Hockney, R. .; Goel, S. .; Eastwood, J. . Quiet High-Resolution Computer Models of a Plasma. *J. Comput. Phys.* **1974**, *14* (2), 148–158.

(58) Hess, B.; Bekker, H.; Berendsen, H. J. C.; Fraaije, J. G. E. M. LINCS: A Linear Constraint Solver for Molecular Simulations. *J. Comput. Chem.* **1997**, *18* (12), 1463–1472.

(59) Bussi, G.; Donadio, D.; Parrinello, M. Canonical Sampling through Velocity Rescaling.

J. Chem. Phys. **2007**, *126* (1), 014101.

(60) Parrinello, M.; Rahman, A. Polymorphic Transitions in Single Crystals: A New Molecular Dynamics Method. *J. Appl. Phys.* **1981**, *52* (12), 7182–7190.

(61) Darden, T.; York, D.; Pedersen, L. Particle Mesh Ewald: An N ·log(N) Method for Ewald Sums in Large Systems. *J. Chem. Phys.* **1993**, *98* (12), 10089–10092.

(62) Kollman, P. A.; Massova, I.; Reyes, C.; Kuhn, B.; Huo, S.; Chong, L.; Lee, M.; Lee, T.; Duan, Y.; Wang, W.; et al. Calculating Structures and Free Energies of Complex Molecules: Combining Molecular Mechanics and Continuum Models. *Acc. Chem. Res.* **2000**, *33* (12), 889–897.

(63) Nguyen, T. T.; Mai, B. K.; Li, M. S. Study of Tamiflu Sensitivity to Variants of A/H5N1 Virus Using Different Force Fields. *J. Chem. Inf. Model.* **2011**, *51* (9), 2266–2276.

(64) Ngo, S. T.; Li, M. S. Curcumin Binds to Aβ 1–40 Peptides and Fibrils Stronger Than Ibuprofen and Naproxen. *J. Phys. Chem. B* **2012**, *116* (34), 10165–10175.

(65) Thai, N. Q.; Tseng, N.-H.; Vu, M. T.; Nguyen, T. T.; Linh, H. Q.; Hu, C.-K.; Chen, Y.-R.; Li, M. S. Discovery of DNA Dyes Hoechst 34580 and 33342 as Good Candidates for Inhibiting Amyloid Beta Formation: In Silico and in Vitro Study. *J. Comput. Aided. Mol. Des.* **2016**, *30* (8), 639–650.

(66) Still, W. C.; Tempczyk, A.; Hawley, R. C.; Hendrickson, T. Semianalytical Treatment of Solvation for Molecular Mechanics and Dynamics. *J. Am. Chem. Soc.* **1990**, *112* (16), 6127–6129.

(67) Jurrus, E.; Engel, D.; Star, K.; Monson, K.; Brandi, J.; Felberg, L. E.; Brookes, D. H.; Wilson, L.; Chen, J.; Liles, K.; et al. Improvements to the APBS Biomolecular Solvation Software Suite. *Protein Sci.* **2018**, *27* (1), 112–128.

(68) Duan, L.; Liu, X.; Zhang, J. Z. H. Interaction Entropy: A New Paradigm for Highly Efficient and Reliable Computation of Protein–Ligand Binding Free Energy. *J. Am. Chem. Soc.* **2016**, *138* (17), 5722–5728.

(69) Laskowski, R. A.; Swindells, M. B. LigPlot+: Multiple Ligand–Protein Interaction Diagrams for Drug Discovery. *J. Chem. Inf. Model.* **2011**, *51* (10), 2778–2786.

(70) Redfield, C.; Dobson, C. M. Sequential Proton NMR Assignments and Secondary Structure of Hen Egg White Lysozyme in Solution. *Biochemistry* **1988**, *27* (1), 122–136.

For table of content only